

# East Asia Reanalysis System (EARS)

Jinfang Yin<sup>1</sup>, Xudong Liang<sup>1</sup>, Yanxin Xie<sup>1</sup>, Feng Li<sup>1</sup>, Kaixi Hu<sup>2</sup>, Lijuan Cao<sup>2</sup>,  
Feng Chen<sup>3</sup>, Haibo Zou<sup>4</sup>, Feng Zhu<sup>5</sup>, Xin Sun<sup>5</sup>, Jianjun Xu<sup>6</sup>, Geli Wang<sup>7</sup>, Ying Zhao<sup>8</sup>,  
5 and Juanjuan Liu<sup>7</sup>

<sup>1</sup>The State Key Laboratory of Severe Weather, Chinese Academy of Meteorological  
Sciences, Beijing 100081, China

<sup>2</sup>National Meteorological Information Center, China Meteorological Administration,  
10 Beijing 100081, China

<sup>3</sup>Zhejiang Institute of Meteorological Sciences, Hangzhou 310008, China

<sup>4</sup>Key Laboratory of Poyang Lake Wetland and Watershed Research Ministry of  
Education, Jiangxi Normal University, Nanchang 330022, China

<sup>5</sup>Inner Mongolia Meteorological Observatory, Inner Mongolia Hohhot 010051, China

15 <sup>6</sup>College of Oceanography and Meteorology, Guangdong Ocean University, Zhanjiang  
524088, China

<sup>7</sup>Institute of Atmospheric Physics, Chinese Academy of Sciences, Beijing 100029,  
China

20 <sup>8</sup>School of Mathematics, Nanjing University of Aeronautics and Astronautics, Nanjing  
211106, China

Submitted to *Earth System Science Data (ESSD)*

December 2022

*Correspondence to:* Xudong Liang (liangxd@cma.gov.cn)

25 **Abstract.** Reanalysis data plays a vital role in weather and climate study, as well as  
meteorological resource development and application. In this work, the East Asia Reanalysis  
System (EARS) was developed using the Weather Research and Forecasting (WRF) model  
and the Gridpoint Statistical Interpolations (GSI) data assimilation system. The regional  
reanalysis system is forced by the European Centre of Medium-Range Weather Forecasts  
30 (ECMWF) global reanalysis EAR-Interim data at 6-h intervals; and hourly surface  
observations are assimilated by the Four-Dimension Data Assimilation (FDDA) scheme  
during the WRF model integration; upper observations are assimilated in a three-dimensional  
variational data assimilation (3D-VAR) mode at analysis moment. It should be highlighted  
that many of the assimilated observations have not been used in other reanalysis systems. The  
35 reanalysis runs from 1980 to 2018, producing a regional reanalysis dataset covering East Asia  
and surrounding areas at 12-km horizontal resolution, 74 sigma levels, and 3-hour intervals.  
Finally, an evaluation of EARS has been performed with the respect to the root mean square  
error (RMSE), based on the 10-year (2008-2017) observational data. Compared to the global  
reanalysis data of the EAR-Interim, the regional reanalysis data of the EARS are closer to the  
40 observations in terms of RMSE in both surface and upper-level fields. The present study  
provides evidence for substantial improvements seen in EARS compared to the ERA-Interim  
reanalysis fields over East Asia. The study also demonstrates the potential use of the EARS  
data for applications over East Asia and proposes further plans to provide the latest reanalysis  
in real-time operation mode. Simple data and updated information are available on Zenodo at  
45 <https://doi.org/10.5281/zenodo.7404918> (Yin et al., 2022), and the full datasets are publicly  
accessible on the Data-as-a-Service platform of China Meteorological Administration (CMA)  
at <http://data.cma.cn>.

**Keywords:** Regional reanalysis, East Asia, Data assimilation, Multiple observations

## 50 **1. Introduction**

The East Asia Reanalysis System (EARS) project was launched by the China Meteorological Administration (CMA) in late 2014. It aimed to build a regional reanalysis system that can assimilate as much as possible multi-source observational datasets, and to establish a long-term high-resolution regional atmospheric reanalysis, which is high quality for mesoscale weather, regional climate, environment studies, and other applications. This paper is to report the progress of the project, including the used numerical model, data assimilation, observations, and preliminary achievements. Thus, the major objectives of the present study are to (i) introduce the work we have already done; (ii) help understand and use the EARS reanalysis products; and (iii) provide guidance for repeating and extending the work in the future.

Atmospheric reanalysis data, which may serve as alternative data to actual observations, play an important role in weather and climate studies, including numerical model validation. In the past several decades, a series of atmospheric reanalysis products were produced with different goals (Wright et al., 2019); some have been widely used in theoretical studies and applied to weather and climate research to improve prediction skills and reduce hazard risks. With the ongoing development of atmospheric sciences, high-resolution atmospheric reanalysis data are much needed. In view of this demand, a large number of high-resolution regional reanalysis products have been produced for various parts of the world (e.g., Mesinger et al., 2006; Jakob et al., 2017; Vidal et al., 2010; Usui et al., 2017; Yang et al., 2022). However, little attention has been paid to East Asia, although China's first generation of global atmospheric reanalysis (CRA40) was released recently, with a horizontal resolution of approximately 34 km and a temporal resolution of 6 h. Only low-resolution global reanalysis products have been used for the region, including the National Centers for Environmental Prediction-Department of Energy Reanalysis version 2 (NCEP2) (Kanamitsu et al., 2002), the

75 European Centre of Medium-Range Weather Forecasts (ECMWF) Reanalysis-Interim  
(ERA-Interim) (Dee et al., 2011), the Japanese 55-year Reanalysis (JRA55) (Kobayashi et al.,  
2015), and the Modern-Era Retrospective Analysis for Research and Applications version 2  
(MERRA2) (Gelaro et al., 2017). More recently, the ECMWF released the fifth generation of  
its atmospheric reanalysis (ERA5) (Hersbach et al., 2020), replacing the ERA-Interim; it is a  
80 global atmospheric reanalysis with a horizontal resolution of 0.25 degrees. Although these  
global reanalysis systems have achieved great progress, their products were developed for  
global coverage. They have limited regional usage due to low spatial and temporal resolution  
(Chen et al., 2014). Most importantly, multiple observations over East Asia were not included  
in these global reanalysis products. Consequently, the global reanalysis products are  
85 inadequate for studying characteristics of local weather and climate in East Asia, such as  
strong rainfall in the warm sector in southern China during the period from April to June (the  
so-called pre-summer rainy season) (Chen et al., 2014). In view of the above-mentioned  
inherent issues, it is highly imperative to develop a high spatiotemporal-resolution reanalysis  
product for East Asia.

90 Several regional atmospheric reanalysis datasets were produced in the past two decades,  
such as the North American Regional Reanalysis (NARR) (Mesinger et al., 2006), the  
High-resolution Regional Reanalysis for the European Coordinated Regional Downscaling  
Experiment (CORDEX) (Bollmeyer et al., 2015; Bach et al., 2016), the Arctic System  
Reanalysis (ASR) (Bromwich et al., 2017), the Bureau of Meteorology Atmospheric  
95 high-resolution Regional Reanalysis for Australia (BARRA-R) (Jakob et al., 2017),  
high-resolution regional reanalysis of Japan (NHM-LETKF) (Fukui et al., 2018), and the  
regional reanalysis of Indian Monsoon Data Assimilation and Analysis (IMDAA) (Mahmood  
et al., 2018). These data have been widely used for regional weather and climate studies.  
Recently, Yang et al. (2022) developed 10-year (2010-2019) regional reanalysis, focusing on

100 the Korean Peninsula and its surrounding areas only. With the same objective, the CMA  
planned a project, intending to produce a high-resolution regional atmospheric reanalysis  
data with high quality for mesoscale weather study and regional climate analysis over East  
Asia. For this purpose, the EARS was launched in late 2014 and a 39-year (1980-2018)  
reanalysis dataset is now available to the public.

105 This is our first open documentation of the project, on the basis of several progress  
reports (e.g., Liang et al., 2020; Yin et al., 2019), which briefly describes the EARS and  
documents its performance. It includes the numerical model set, data assimilation method,  
assimilated observational datasets, and preliminary results. In section 2, we describe the  
EARS system and the data used. In section 3, we present the preliminary results of a 10-year  
110 (2008-2017) reanalysis dataset with validation. Finally, a summary and discussion are  
provided in section 4, along with future activities and plans.

## **2. East Asia Reanalysis System and Data Used**

### **2.1 System Setup**

The EARS is established based on the Advance Research Weather Research and  
115 Forecasting (WRF version 3.9.1) model (Skamarock et al., 2008) and the Gridpoint Statistical  
Interpolations (GSI) data assimilation system (Hu et al., 2018). To improve the model  
performance in East Asia, a series of experiments were launched for dynamic and physical  
options. At present, the GIS runs in a three-dimensional variational data assimilation  
(3D-VAR) mode, and much attention has been paid to the effect of assimilating each category  
120 of observations. To date, the EARS works continuously in a 39-year run, with a cold start at  
the interval of six hours.

In the EARS (Fig. 1), the WRF-ARW model grid spacing is 12 km, which covers a large  
domain of an area of 10,800 km  $\times$  9,120 km (with 900  $\times$  760 grid points); and it is centered at

(100°E, 38°N). A total of 74 sigma levels is used in the vertical, with the model top fixed at  
125 10 hPa. The model terrain is interpolated from the 30-arc-second USGS GMTED2010; and  
the land use fields are interpolated from 21-class MODIS datasets. The model physics  
schemes used include the following: (i) the Kain (2004) cumulus parameterization scheme; (ii)  
the new Thompson microphysics scheme (Thompson et al., 2008); (iii) the rapid radiative  
transfer model (Iacono et al., 2008) for both shortwave and longwave radiative flux  
130 calculations; (iv) the Yonsei University (YSU) Planetary Boundary Layer (PBL) scheme  
(Hong et al., 2006); (v) the revised MM5 Monin-Obukhov similarity scheme for the surface  
layer (Janjić, 1994), and (vi) the Noah-MP land-surface scheme (Niu et al., 2011). It should be  
emphasized that the model set was optimized via a series of experiments covering various  
weather phenomena and continuous simulations (e.g., Zhang et al., 2016; Li et al., 2018; Yin  
135 et al., 2014; Yin et al., 2020).

A schematic illustrating the flow of analysis steps of the EARS is shown in Fig. 2. The  
WRF model integrates for 12 hours in every cold start, starting at 0000, 0600, 1200, and 1800  
UTC, with hourly outputs. The ERA-Interim 0.79-degree reanalysis data at 6-h intervals are  
utilized as initial and boundary conditions for the cold run. Please refer to Dee et al. (2011)  
140 for detailed information on the ERA-Interim reanalysis data. At the model's initial time, the  
upper-level (sounding and aircraft) observations are assimilated with the GSI system in  
3D-VAR mode. During the model integration, the Four-Dimension Data Assimilation (FDDA)  
functions are activated by performing surface observation nudging (Reen, 2016). The required  
analysis data for the FDDA are obtained through the WRF's preprocessing OBSGRID module  
145 (Wang et al., 2017), using the hourly surface observations after performing data quality  
control, which includes temperature, relative humidity, and horizontal winds. More  
specifically, observation nudging is a type of FDDA wherein artificial tendency terms are  
introduced during the model integration (Reen, 2016). Since it is applied at every time step,

nudging is a continuous form of data assimilation. Therefore, observations in the model  
150 integration time window can be well ingested. Generally speaking, the differences between  
the WRF model and observation are utilized to create innovations. Then, the innovations are  
multiplied by various factors and added to model tendency equations. It should be noted that  
observation nudging is affected by the uncertainty of the observations. Therefore, surface  
observations are strictly quality controlled by the OBSGRID module (Wang et al., 2017).

155 The model outputs in the first six hours are considered the spin-up process, and thus not  
used for research. The model outputs at the ninth and twelfth hours are used as the first guess  
of the GSI; and the upper-level observations are assimilated in a 3D-VAR mode. The  
upper-level observations include sounding, aircraft observation, and cloud-derived wind  
vector. The composited radar reflectivity is ingested by the way of cloud analysis to produce  
160 the final reanalysis data. Note that model hourly outputs are also available. Unlike a  
continuously operating global reanalysis system, the EARS conducts a cold start every six  
hours, and the WRF model integrates 12 hours for each run. Accordingly, the model outputs  
from the sixth to twelfth hours are used to produce hourly precipitation during the WRF  
model integration. Before generating long-term reanalysis, the EARS was validated by  
165 continuous simulations of the year 2014. The results indicated that the EARS performed  
better in terms of atmospheric variables, and provided more mesoscale details than the  
large-scale ERA-Interim reanalysis (used as background in the EARS), and its outputs can be  
used for developing a long-term reanalysis product.

## **2.2 Assimilated Data**

170 Various categories of observational data used in the EARS are listed in Table 1. The  
National Meteorological Information Center (NMIC) of CMA archives all observational  
datasets after performing strict data quality control. Generally speaking, several steps were  
used to prepare the input observations. Firstly, the duplicate (in time and location) data reports

were merged. Secondly, all the ground-based observations, including were checked by  
175 climatic cut-off values and variation ranges. Besides, internal consistency between  
meteorological elements and temporal consistency were carried out. Moreover, soundings  
were examined based on hydrostatic assumption, temperature lapse rate, and horizontal wind  
shear. The observational data are publicly accessible at <http://data.cma.cn/> (last access 8 Jan  
2023). In particular, the traditional observational datasets have been greatly improved by  
180 merging multiple data sources, which are officially released by the NMIC. Note that many of  
the datasets were not shared publicly before. Figure 3 shows spatial distributions of  
radiosonde and radar observations, surface observations over land, and surface observations  
over the ocean. Note that the aircraft and satellite (cloud-derived wind vector) observations  
are not presented due to irregular moving trajectories depending on time and space.

185 Previous studies (e.g., Kawai et al., 2017; Benjamin et al., 2010; Lee et al., 2019; Rabier  
et al., 2009; Ingleby et al., 2016) have confirmed that numerical model performances were  
enhanced by assimilating radiosonde observations globally. Figure 4 shows the radiosonde  
observations assimilated in the EARS, which has been greatly improved by combining  
datasets from various databases and employing more observational data sources from China.  
190 It can be seen that the counts of radiosonde observations show slight variation from 1980 to  
2000, and then increase obviously, almost doubled by 2018. In addition to conventional  
observations shared in the Global Communication System (GTS) of World Meteorological  
Organization (WMO), another 33 radiosonde stations in China are incorporated. Most  
importantly, more vertical-level observations are included by merging logs of old records.  
195 Taking the radiosonde observations of Beijing station at 0000 UTC 1 July 2016 as an example  
(Fig. 5), the merged radiosonde observations show more detailed vertical structures,  
compared to those in the Integrated Global Radiosonde Archive (IGRA) version 2, which is  
used in the National Center for Atmospheric Research (NCAR) global reanalysis of the



Climate Forecast System Reanalysis (CFSR). Besides, radiosonde observations at both 0600  
200 and 1800 UTC are used (Fig. 4a,c), although the observations are discontinuous and much  
fewer than those at 0000 and 1200 UTC (Fig. 4b,d). Moreover, radiosonde observations from  
field experiments are used, including those from the Third Tibetan Plateau Atmospheric  
Scientific Experiment (TIPEX-III) (Zhao et al., 2018), the Southern China Monsoon Rainfall  
Experiment (SCMREX) (Luo et al., 2017), among others. Note that these supplementary  
205 radiosonde observations were not utilized in any global reanalysis system outside of China.  
Overall, the number of radiosonde observations assimilated in the EARS has increased  
significantly after combining several sources, especially from 2000 to 2018.

Previous studies (e.g., Mirza et al., 2016; James et al., 2020) indicated that assimilating  
aircraft observations was beneficial for numerical modeling. The aircraft observations used in  
210 the EARS are provided by the NMIC after quality control (Liao et al., 2021), which is a new  
product by integrating nine different data sources into the Integrated Global Meteorological  
Observation Archive from Aircraft (IGMOAA). Adding the datasets from the Chinese  
Aircraft Meteorological Data Relay (AMDAR), the observation count has increased  
significantly, compared to that of the IGMOAA. The integrated data were officially released  
215 by the NMIC and are updated in real-time at the Data-as-a-Service platform  
(<http://data.cma.cn/>). Generally speaking, aircraft observations were rare in the early days;  
and these observations have increased greatly from  $2 \times 10^3$  in 2005 to  $7 \times 10^3$  in 2018 (Fig. 6).  
Although the aircraft observations are hourly, there are large differences at different moments  
of the day. One can see that the count of aircraft observations in the daytime is much larger  
220 than that in the nighttime, though the count of aircraft observations in the nighttime has  
slightly increased since 2005.

For surface observations over land (Fig. 3b and Fig. 7a), besides those from the National  
Centers for Environmental Prediction (NCEP) Global Data Assimilation System (GDAS) and

the National Climatic Data Center (NCDC) Integrated Surface Database (ISD), more than  
225 2440 surface observations from the CMA are added. Detailed processing of the datasets can  
be found in Jiang et al. (2021). Note that only a small portion (less than 300 stations in the  
early days and nearly 400 stations at present) of the surface observations is shared in the GTS.  
The observations over the sea surface are combined with the International Comprehensive  
Ocean-Atmosphere Data Set (ICOADS) (Fig. 3c). After the combination, the ocean-based  
230 observation count used in the EARS increases by approximately 32% in total, compared to  
the ICOADS. As shown in Fig. 7b, the surface observations have increased significantly,  
especially since 2000. All the hourly surface observations (over land and ocean) are further  
quality controlled by using the OBSGRID module provided by the WRF Variational Data  
Assimilation (WRFDA); and the outputs in ASCII format are used for observation nudging  
235 during the WRF model integration. We pointed the readers to Skamarock et al. (2008) for  
more details. Similarly, all the upper-level traditional observational datasets are quality  
controlled by using the OBSPROC module, and then written in the prepBUFR format for GSI  
assimilation in a 3D-VAR mode.

One of the main features of the EARS is its emphasis on radar data assimilation. All  
240 weather radar observations over China are used in the EARS (Fig. 3d). Radar observations  
have increased rapidly from 80 stations in 2008 to over 190 stations in 2018 (Fig. 8). Note the  
radar observations show obvious seasonal various because most of the radars are out of  
service in cold seasons. To obtain high-quality-controlled radar observational data, much  
attention has been paid to the preprocessing of raw radar data. A major issue of the radar  
245 observations is the non-meteorological echo, which has direct influences on the cloud  
hydrometeors in the GSI cloud analysis processes. In view of this issue, much effort has been  
devoted to removing isolated non-meteorological echoes and ground clutters from the radar  
data (Zou et al., 2018), which makes quality-controlled radar data more accurate (Wu et al.,

2018). After quality control, all radar observations at the same time are utilized to generate  
 250 mosaic products in BUFR format, which can be inserted into the GSI cloud reanalysis module.  
 Detailed information about radar data processing and remapping can be found in Zou et al.  
 (2014). The cloud analysis module in the GSI came from the Advanced Regional Prediction  
 System (ARPS) (Hu and Xue, 2007), and can be further traced to the Local Analysis and  
 Prediction System (LAPS) (Albers et al., 1996). In fact, quality-controlled radar observations  
 255 are also an important part of the reanalysis data, which can be used for weather and climate  
 studies, as well as numerical model validation. Despite considerable effort expended in  
 processing radial wind, the radial wind has been not assimilated at present as more work is  
 required.

Another feature is the application of the cloud-derived wind vector datasets from  
 260 Fengyun-2 geostationary meteorological satellites. The cloud-derived wind vector appears  
 with a count of nearly  $6.0 \times 10^4$  (Fig. 9). Note that the data have been strictly quality controlled  
 and widely applied in daily operational numerical weather prediction in China; thus these  
 datasets can be applied directly in the EARS.

265 **Table 1.** Observational data used in EARS. Those data are publicly accessible at  
<http://data.cma.cn/> (last access 8 Jan 2023)

<b>Data</b>	<b>Variable</b>	<b>Starting year</b>
Radiosonde	Pressure, temperature, wind, and moisture	1980
Aircraft	Temperature and wind	1980
Surface <sup>1</sup>	Pressure, temperature, wind, and moisture	1980
Radar	Radar reflectivity	2008
Satellite	Cloud-derived wind vector	2008

<sup>1</sup> Including the surface observations over ocean.

### 2.3 Validation Data and Method

The performance of the EARS is assessed by comparing it with observations and with  
270 the large-scale forcing of the ERA-Interim reanalysis (used as the background of the EARS).  
A 10-year good quality and stable quantity of observations are selected for the assessment.  
For comparison with station observations, results from the EARS and ERA-Interim are  
interpolated onto the stations using the nearest neighbor interpolation via the Model  
Evaluation Tools (MET), which is developed by the Developmental Testbed Center (DTC) of  
275 the U.S. (Newman et al., 2022). Following the operational model evaluations of the CMA, we  
use a total of 2,423 surface observational stations as the reference for the reanalysis data  
validation. The observations over the Qinghai-Tibet Plateau and its surrounding areas are  
much sparser, compared to those over the other regions (Fig. 10a). Similarly, a total of 120  
radiosonde data over China are used to evaluate high-level variables (Fig. 10b). As has been  
280 stated above, the radiosonde observations are mainly obtained at 0000 UTC and 1200 UTC,  
and the measurements include temperature, (relative) humidity (or dew-temperature), air  
pressure, horizontal wind speed, and direction. It should be noted that the present validation is  
based on the observations from CMA. Although the EARS covers a large area, only limited  
observations out of China were obtained by the GTS. Comparatively speaking, the density of  
285 observations is much higher in China than that out of China. Besides, the performance of  
observations in China is at a comparable level because of the same (at least equivalent)  
observational instruments and methods. Moreover, the observations in China were quality  
controlled using the same methods. Therefore, the observations in China were used in the  
validation. We welcome more validation from others with observations outside of China as  
290 much as possible.

The quality of the regional reanalysis is also compared to one-month (July 2016)  
continuous radiosonde observational data, which were obtained from a field experiment in the

central Taklimakan Desert, Xinjiang Uygur Autonomous Regions, China. The central Taklimakan Desert is far from other observation sites, where the assimilated observations have little influence on the reanalysis data. Note that these data have not been applied to any weather forecasting or reanalysis systems (including global and regional systems), which should be an excellent source of independent observations (Huang et al., 2021). The radiosonde observational station (marked with a black star in Fig. 10b) is located at (83.63°E, 39.04°N), 1,099.3 m above the sea level. The radiosonde observational data were collected four times at 0000, 0600, 1200, and 1800 local standard time (LST, = UTC + 6) a day in July 2016, using the Global Positioning System (GPS)-based radiosonde. One of the advantages of the radiosonde observation is its high vertical resolution, which is achieved by high frequency (at intervals of one second) data acquisition during balloon ascending.

To assess the new EARS data, we compare them with surface and radiosonde observations in terms of root mean square error (RMSE), given by

$$RMSE = \sqrt{\frac{1}{N} \sum_{i=1}^N (F_i - O_i)^2}, \quad (1)$$

where  $N$  is the total number of all observations;  $F_i$  and  $O_i$  denote reanalysis data and observation, respectively.

We use RMSE(EARS) and RMSE(ERA-I) to represent the RMSEs for the regional EARS and global ERA-Interim, respectively. The fractional percentage improvement ( $I$ ) of the RMSE can be defined as follows:

$$I(\%) = \frac{RMSE(ERA-I) - RMSE(EARS)}{RMSE(ERA-I)} \times 100\%. \quad (2)$$

Accuracy is perhaps the most widely used objective validation method for quantitative precipitation forecasts. Following the MET verification measures for categorical (dichotomous) variables, we employ a table of  $2 \times 2$  contingency (Table 2). The accuracy of precipitation forecast is defined by

$$Accuracy = \frac{hits + correct\ negatives}{total}. \quad (3)$$

The accuracy ranges from 0 to 1, and a perfect forecast would have an accuracy of 1.

**Table 2.** Contingency table for categorical (dichotomous) variables.

		observation		
		yes	no	total
reanalysis	yes	hits	false alarms	forecast yes
	no	misses	correct negatives	forecast no
	total	observed yes	observed no	total

320

### 3. Results

#### 3.1 Performance of Surface Field

Figure 11 compares 10-year-averaged RMSEs of surface variables from the EARS and ERA-Interim using box-percentile plots. For the EARS, the averaged RMSEs of surface pressure ( $P$ ), temperature ( $T$ ), specific humidity ( $Q$ ), zonal wind ( $U$ ), meridional wind ( $V$ ), and wind speed ( $WS$ ) are 14.11( $\pm$ 19.22) hPa, 2.05( $\pm$ 1.43) $^{\circ}$ C, 1.18( $\pm$ 0.28) g kg $^{-1}$ , 1.76( $\pm$ 0.69) m s $^{-1}$ , 1.95( $\pm$ 0.63) m s $^{-1}$ , and 2.06( $\pm$ 0.58) m s $^{-1}$ , respectively. The ERA-Interim has larger averaged RMSEs of  $P$ ,  $T$ ,  $Q$ ,  $U$ ,  $V$ , and  $WS$ , which are 24.34( $\pm$ 27.17) hPa, 2.25( $\pm$ 1.43) $^{\circ}$ C, 1.33( $\pm$ 0.35) g kg $^{-1}$ , 1.98( $\pm$ 0.58) m s $^{-1}$ , 2.35( $\pm$ 0.70) m s $^{-1}$ , and 2.42( $\pm$ 0.51) m s $^{-1}$ , respectively. In terms of the RMSE, the EARS performs much better, with respective improvement percentages of 42.01%, 8.82%, 11.28%, 11.37%, 16.96%, and 14.75% for  $P$ ,  $T$ ,  $Q$ ,  $U$ ,  $V$ , and  $WS$ , respectively. Generally speaking,  $P$  has the largest improvement, followed by  $V$ ,  $U$ , and  $Q$ ; and  $T$  has the smallest improvement. Similarly, the 25th, 50th, and 75th percentiles show obvious improvements.

335 In terms of the RMSE, we have noted that the EARS shows an obvious improvement in

the surface meteorological fields over East Asia, compared to it's the ERA-Interim (Fig. 11). According to the statistical results,  $P$  has the largest improvement percentage of the RMSE, followed by  $V$ ; and  $T$  has the smallest improvement. The smaller RMSE is mainly attributable to the data assimilation of a large number of observations. Note that the optimized WRF model, focusing on East Asia with a high horizontal resolution of 12 km and 74 sigma levels in the vertical, is also beneficial to the smaller RMSE. As has been stated above, the WRF model was tested and verified in various aspects by paying attention to dynamic and physical options, and to observation nudging parameters (Yin et al., 2018). According to our previous tests with the optimized WRF model, the downscaling results performed better than the ERA-Interim, which provides good background conditions for the GSI data assimilation and the subsequent reanalysis data. Previous studies (e.g., Andrys et al., 2015; Gao et al., 2022; Qiu et al., 2017) also indicated that significant performances have been gained in WRF downscaling at a high resolution.

Figure 12 shows spatial distributions of the averaged RMSEs of  $P$  for the EARS and ERA-Interim, and for their differences. Clearly, the spatial distribution for the EARS is similar to that of the ERA-Interim. Given the spatial distribution, there is a smaller RMSE over eastern China, which is beneficial from the ingestion of dense surface observations. Note that the higher resolution of the complex terrain over western China has positive contributions to the model results, except for limited observations over this region. More specifically, both EARS and ERA-Interim show large RMSEs over western China, especially along the east side of the Qinghai-Tibet Plateau. The spatial distributions for other surface variables are also generated, although there are not presented here. Please refer to the supplementary for more results. In general, the EARS has similar improvements to  $P$  in  $T$ . Concerning  $Q$ , both EARS and ERA-Interim have obvious RMSEs over southern China, which may be related to a large amount of available water vapor in this region. The EARS shows a similar spatial distribution

of RMSE of  $U$  to that of the ERA-Interim, while obvious differences can be found in the RMSE of  $V$ . A large RMSE belt of  $U$  is in the northeast toward the Tibet Plateau. The EARS reduces RMSE in  $V$  significantly, indicating that the quality of  $V$  is improved considerably. The EARS alleviates the RMSE over values  $2.5 \text{ m s}^{-1}$  at most stations. Note that the EARS has larger RMSEs in the wind field (both  $U$  and  $V$ ) over western China than the ERA-Interim. This may be related to complicated dynamics associated with the Tibet Plateau, land processes, or/and poor quality of observations over this region; and attention is required to understand the shortcoming. For  $WS$ , the improvement shows a similar pattern to that in  $V$ . In terms of RMSE, the EARS performs better than the ERA-Interim at most stations, although the EARS has poor quality at some stations.

### 3.2 Upper-Level Fields

Figure 13 shows the mean RMSEs of vertical profiles of  $U$ ,  $V$ ,  $T$ , and  $Q$ , verified against 120 radiosonde observations over China during 2008-2017 (Fig. 10b). Generally speaking, the EARS shows much smaller RMSEs than the ERA-Interim at all levels, although both show similar vertical distributions. The RMSEs for the ERA-Interim are nearly twice as large as those of the EARS, except for the RMSEs of  $Q$  at the upper levels. More specifically, the RMSEs of  $U$  and  $V$  for the EARS are nearly  $1 \text{ m s}^{-1}$  throughout the vertical column, while those of the ERA-Interim are mostly larger than  $2 \text{ m s}^{-1}$ . Also, the RMSEs of  $U$  and  $V$  for the EARS show slight variation in vertical, while the RMSEs of ERA-Interim are large at the lower and upper levels and small at the middle levels. As for the RMSEs of  $T$ , the RMSEs of the EARS are within  $0.9^\circ\text{C}$ ; and the RMSEs of the ERA-Interim are less than  $1.5^\circ\text{C}$ . Both reanalysis products show large RMSEs at the lower level near the ground; and the RMSEs for  $T$  decrease first with increasing height, bottomed out near 400 hPa. The second-largest RMSEs for  $T$  occur at the higher level of 100 hPa. The large RMSEs for  $T$  at the upper levels mainly result from limited radiosonde observations. Besides, the interactions between the



troposphere and stratosphere may have some impact on the accuracy of the reanalysis products. The RMSEs for  $Q$  decrease rapidly with increasing height and approach zero near 200 hPa, which corresponds to the decrease of moisture content from the bottom to up. It should be pointed out that the small RMSEs at the upper levels result from a very low value of  $Q$ , rather than from having a good performance at these levels. In view of the vertical profiles of the EARS verifying against radiosonde observations given in Fig. 13, the EARS is considerably better than the ERA-Interim. The RMSEs for EARS are almost half as small as that of the ERA-Interim. The RMSEs of  $U$ ,  $V$ , and  $T$  for the EARS are considerably smaller than those of the ERA-Interim. At upper levels above 500 hPa, the RMSEs of  $Q$  for both EARS and ERA-Interim are similar in magnitude, while the former shows a smaller value than the latter. As stated in Mesinger et al. (2006), the reanalysis data are influenced by both the estimate of the background and observation error covariances.

### 3.3 Rainfall

Despite several objective verification methods for modeling quantitative rainfall amounts, systematic assessment of simulated rainfall performance remains difficult. Consequently, a simple comparison between the EARS and ERA-Interim is given here in terms of the accuracy of 3-h accumulated rainfall. Please refers to Yang et al. (2023) for detailed analyses of the simulated rainfall properties of the EARS. Figure 14 shows the accuracy of 3-h rainfall for both EARS and ERA-Interim. Although the accuracy shows slight diurnal variation, both EARS and ERA-Interim have high averaged accuracies of over 0.5 and show good performances from early morning (2100 UTC) to the midday on next day (0300 UTC). The EARS has higher rainfall accuracy than the ERA-Interim at all times. For an overview (i.e., mean), the EARS provides a higher total mean accuracy of 0.61, with 0.56 for the ERA-Interim. Note that the improvements vary from 4.53% to 16.18%, with the averaged improvement percentage of the accuracy being 8.99%. We also calculated the equitable threat

score for 3-h accumulated rainfall (not shown). For rainfalls above 20.0 mm, the EARS is much better than the ERA-Interim, indicating that the EARS has better capability to reproduce heavy rainfall over East Asia, especially for 3-h accumulated rainfall that is over 50 mm. Note that the ERA-Interim cannot capture 3-h accumulated rainfall that is over 70 mm, which may be caused by the global model's low resolution of nearly 79 km.

Figure 15 shows the spatial distribution of averaged 3-h accumulated rainfall accuracy for the EARS and ERA-Interim in 2008-2017. Clearly, both EARS and ERA-Interim have high forecast capability for precipitation over central China with rainfall accuracy of over 0.6, followed by southern and eastern China (Figs. 15a, b). The low accuracy (less than 0.4) mainly appears in western China, especially over the Qinghai-Tibet Plateau. The results are consistent with previous studies and with operational predictions (e.g., Mao et al., 2010; Zhang et al., 2021; Zhao et al., 2018). In general, the EARS has better performance on the 3-h scale at most stations than the ERA-Interim (Fig. 15c), although the EARS has less accuracy at some stations. The EARS with more local observations is probably the main reason for its better performance; and the benefit of the optimized WRF model with the high resolution of 12 km may be another reason. The results indicate that the EARS would be more suitable for investigating precipitation over East Asia.

### **3.4 Features in Lower Levels over Central Taklimakan Desert**

Figure 16 shows the diurnal variation of observed and simulated vertical thermal structures in the lower levels (0.6 km above the ground). From the observations, obvious transitions exist in the thermal structure. More specifically, there is an inversion layer near the surface in the nighttime, while a sub-adiabatic or superadiabatic layer occurs in the daytime. The transition, from stable to convective and back to stable condition, is consistent with the diurnal variation of solar radiation (Yin et al., 2021). In general, both the EARS and ERA-Interim are able to reproduce similar diurnal transitions as in the observations. Although

there are some differences between the reanalysis products and observations, the transitions, from stable to convective and back to stable condition, are consistent with the observations. Specifically, the EARS is closer to the observations, compared to the EAR-Interim. For instance, the EARS captures the obvious inversion at 0600 local standard time (LST), while  
440 the ERA-Interim underestimates the inversion.

Figure 17 compares the averaged profiles of observed horizontal wind and those of the reanalysis products. An obvious directional shift from northeasterly to westerly appears nearly 2.6 km above the ground on average. In fact, the altitude of the wind directional shift exhibits noticeable diurnal fluctuation, bottomed out at 0600 LST and peaked at 1800 LST with  
445 altitudes near 2.0 and 3.4 km, respectively. Note that the horizontal wind speed decreases and then increases with increasing height due to vertical wind shear. Compared to the observations, both EARS and ERA-Interim capture the principal vertical wind profile patterns over the central Taklimakan Desert. However, the diurnal variation of wind profiles is slightly underestimated by the EARS, while the ERA-Interim completely misses the diurnal  
450 fluctuation. Besides, the ERA-Interim underestimates wind speed near the surface; it seems that the ERA-Interim reanalysis system cannot well describe the near-surface thermodynamic processes.

#### **4. Conclusions and future outlook**

We present a detailed report about the EARS, including 39-year (1980-2018)  
455 high-resolution regional reanalysis datasets over East Asia that show major improvements over the global reanalysis in both spatial resolution and accuracy. The qualities of the reanalysis dataset were verified based on surface observations and radiosonde observations from 2008 to 2017, as well as radiosonde observations from field experiments in July 2016. Regarding resolution, the 12-km grid is much higher than those of global models. For  
460 accuracy, both near-surface and upper-level fields are closer to the observations than the

global reanalysis ERA-Interim.

The EARS is established based on the WRF-ARW model and GSI data assimilation system. To improve the EARS's performance in East Asia, a series of experiments have been conducted for selecting dynamic and physical options. For the GSI, much attention was paid to the improvements of assimilating each category of observations. The EARS started cold runs every day, starting at 0000, 0600, 1200, and 1800 UTC with the ERA-Interim 0.79-degree analysis data at 6-h intervals as initial and boundary conditions. The WRF model was integrated for 12-h each time with hourly outputs; and hourly surface observations were ingested by performing surface observation nudging. The model outputs at the ninth and twelfth hours are used as the first guess of the GSI, and the upper-level observations were assimilated in a 3D-VAR mode and mosaic radar reflectivities were ingested by cloud analysis. To the present, 39-year (1980-2018) reanalysis data have been achieved.

To assess the EARS data, 10-year (2008-2017) data were compared with surface and radiosonde observations in terms of RMSE. The results show substantial improvements in the EARS, compared to the ERA-Interim reanalysis over East Asia. The better performance of the EARS is mainly attributable to the data assimilation of a large number of observations. In addition, the optimized WRF model, focusing on East Asia with a high resolution of 12 km and 74 sigma levels, is also beneficial to the high quality of the EARS. It should be noted that the present validation is based on the observations from CMA. Although the EARS covers a large area, only limited observations were obtained by the Global Communication System (GTS). We welcome more validation from others with observations outside of China as much as possible.

To date, We are fully occupied with EARS development and data generation. The EARS data was verified against both surface and sounding observations. The results were also compared with its parent—the ERA-Interim. At present, comparisons with other global

reanalysis have not been undertaken. As far as we know, the assessment of reanalysis data is a complex and systematic task. Therefore, we expect more scholars to evaluate EARS data from different aspects, such as the performance in reproducing weather systems (e.g., Gong et al., 2022), daily variation in precipitation (e.g., Li et al., 2017), and others, as well as comparisons among different reanalysis (e.g., Yang et al., 2023). In the future, we will further inspect the regional high-resolution data against the observations from the Second Tibetan Plateau Scientific Expedition and Research (STEP) program, in particular using it in high-resolution studies over the East Asian monsoon region. Besides, radar retrieval horizontal wind, which is retrieved by an improved version of the Integrating Velocity-Azimuth Process (IVAP) method (Liang et al., 2019), will be ingested by performing upper-level observation nudging. Most importantly, from 2019 onward, we will shift to using the ERA5 products as initial and boundary conditions for the WRF model. Besides, the intensive surface observations (exceeding 80,000) over China after strict quality control will be introduced in the surface observation nudging. The EARS will run in real-time operation mode to provide the latest reanalysis data with approximately a 5-day lag (depending on the availability of the ERA5 data).

## Appendix A: Abbreviations

**Table A1** List of abbreviations used in the paper.

<b>Abbr.</b>	<b>Term</b>
3D-VAR	Three-dimensional variational data assimilation
AMDAR	Aircraft Meteorological Data Relay
ASR	Arctic System Reanalysis
BARRA-R	Bureau of Meteorology Atmospheric high-resolution Regional Reanalysis for Australia
CMA	China Meteorological Administration
CFSR	Climate Forecast System Reanalysis
CORDEX	Coordinated Regional Downscaling Experiment
CRA40	China's first generation of global atmospheric reanalysis
EARS	East Asia Reanalysis System
ECMWF	European Centre of Medium-Range Weather Forecasts

ERA5	ECMWF fifth generation of its atmospheric reanalysis
ERA-Interim	ECMWF ERA-Interim reanalysis
FDDA	Four-Dimension Data Assimilation
GDAS	Global Data Assimilation System
GSI	Gridpoint Statistical Interpolations
GTS	Global Communication System
ICOADS	International Comprehensive Ocean-Atmosphere Data Set
IGMOAA	Integrated Global Meteorological Observation Archive from Aircraft
IGRA	Integrated Global Radiosonde Archive
IMDAA	Indian Monsoon Data Assimilation and Analysis
ISD	Integrated Surface Database
JRA55	Japanese 55-year Reanalysis
MERRA2	Modern-Era Retrospective Analysis for Research and Applications version 2
MET	Model Evaluation Tools
NARR	North American Regional Reanalysis
NCAR	National Center for Atmospheric Research
NCDC	National Climatic Data Center
NCEP	National Centers for Environmental Prediction
NCEP2	National Centers for Environmental Prediction-Department of Energy Reanalysis version 2
NHM-LETKF	high-resolution regional reanalysis of Japan
NMIC	National Meteorological Information Center (NMIC) of CMA
RMSE	Root mean square error
WMO	World Meteorological Organization
WRF	Weather Research and Forecasting
WRFDA	WRF Variational Data Assimilation

505

### Data Availability

A Digital Object Unique Identifier (DOI: <https://doi.org/10.5281/zenodo.7404918>) is available for the EARS reanalysis data. The 39-year EARS data reported in this work are available at 3-h intervals, starting at 00 UTC from 1980 to 2018. The database format is GRIB version 1 and the total volume of the data files is 54.6 TB. The GRIB files are hosted at the CMA Data-as-a-Service platform (<http://data.cma.cn/>) as their total volume exceeds the volume that could be provided by Zenodo (Yin et al., 2022). Simple data and updated information are available on Zenodo at <https://doi.org/10.5281/zenodo.7404918> (Yin et al., 2022), and the full datasets are publicly accessible on the Data-as-a-Service platform of China Meteorological Administration (CMA) at <http://data.cma.cn>. The data can be obtained in the

510

515

form of a hard disk copy by contacting the authors at present, and will be accessed freely at this location soon. The EARS 3-h data on pressure levels and hourly precipitation data are available in GRIB format, which can be used as a model (e.g., the WRF) forcings. Owing to the large amounts of data, more variables, and datasets on the 74 model (sigma) levels can also be obtained by contacting the authors.

**Author contributions.** X. Liang proposed the main scientific ideas and contributed to radar data processing. J. Yin contributed supplementary ideas and produced the 39-year regional reanalysis and validation. F. Chen and J. Yin developed the reanalysis system, J. Yin, X. Liang, and Y. Xie analyzed the simulations and wrote the manuscript. K. Hu, L. Cao, and F. Li contributed to the preparation of observational datasets and reanalysis management. H. Zou completed the composite radar reflectivity for complex cloud analysis. G. Wang and Y. Zhao launched the simulations for WRF model optimization. J. Liu and J. Xu conducted data assimilation experiments. F. Zhu and X. Sun prepared the programs for validation.

530

**Competing interests.** The authors declare that they have no competing interests.

**Acknowledgments.** This work was conducted by using the PI-Dawning supercomputer system provided by the China Meteorological Administration (CMA). The authors are grateful to the European Centre of Medium-Range Weather Forecasts (ECMWF) for providing the global reanalysis EAR-Interim data (<https://www.ecmwf.int/en/forecasts/datasets/reanalysis-datasets/era-interim>). We thank Dr. Zhiquan Liu at the National Center for Atmospheric Research (NCAR) and Prof. Zijiang Zhou at the National Meteorological Information Center (NMIC) of CMA for their helpful discussions. All the figures are generated by NCAR Command Language (NCL), which is

540

available at <http://dx.doi.org/10.5065/D6WD3XH5> (last accessed on 20 September 2022).

**Financial support.** This study is jointly supported by the National Key Research and Development Program of China (2017YFC1501800), Second Tibetan Plateau Scientific Expedition and Research (STEP) Program (2019QZKK010402), National Natural Science Foundation of China (42075083 and 42192554), National Department Public Benefit Research Foundation (GYHY201506002), and S&T Development Fund of Chinese Academy of Meteorological Sciences (2023KJ047).



## References

- 550 Albers, S. C., McGinley, J. A., Birkenheuer, D. L., and Smart, J. R.: The Local Analysis and  
Prediction System (LAPS): Analyses of Clouds, Precipitation, and Temperature, *Weather  
and Forecasting*, 11, 273-287,  
[https://doi.org/10.1175/1520-0434\(1996\)011<0273:TLAAPS>2.0.CO;2](https://doi.org/10.1175/1520-0434(1996)011<0273:TLAAPS>2.0.CO;2), 1996.
- 555 Andrys, J., Lyons, T. J., and Kala, J.: Multidecadal Evaluation of WRF Downscaling  
Capabilities over Western Australia in Simulating Rainfall and Temperature Extremes,  
*Journal of Applied Meteorology and Climatology*, 54, 370-394,  
<https://doi.org/10.1175/JAMC-D-14-0212.1>, 2015.
- 560 Bach, L., Schraff, C., Keller, J., and Hense, A.: Towards a probabilistic regional reanalysis  
system for Europe: Evaluation of precipitation from experiments, *Tellus A*, 68,  
<https://doi.org/10.3402/tellusa.v68.32209>, 2016.
- 565 Benjamin, S. G., Jamison, B. D., Moninger, W. R., Sahn, S. R., Schwartz, B. E., and Schlatter,  
T. W.: Relative Short-Range Forecast Impact from Aircraft, Profiler, Radiosonde, VAD,  
GPS-PW, METAR, and Mesonet Observations via the RUC Hourly Assimilation Cycle,  
*Monthly Weather Review*, 138, 1319-1343, <https://doi.org/10.1175/2009MWR3097.1>,  
2010.
- Bollmeyer, C., Keller, J. D., Ohlwein, C., Wahl, S., Crewell, S., Friederichs, P., Hense, A.,  
Keune, J., Kneifel, S., Pscheidt, I., Redl, S., and Steinke, S.: Towards a high-resolution  
regional reanalysis for the European CORDEX domain, *Quarterly Journal of the Royal  
Meteorological Society*, 141, 1-15, <https://doi.org/10.1002/qj.2486>, 2015.
- 570 Bromwich, D. H., Wilson, A. B., Bai, L., Liu, Z., Barlage, M., Shih, C. F., Maldonado, S.,  
Hines, K. M., Wang, S. H., Woollen, J., Kuo, B., Lin, H. C., Wee, T. K., Serreze, M. C.,  
and Walsh, J. E.: The Arctic System Reanalysis, Version 2, *Bulletin of the American  
Meteorological Society*, 99, 805-828, <https://doi.org/10.1175/BAMS-D-16-0215.1>, 2017.
- 575 Chen, G., Iwasaki, T., Qin, H., and Sha, W.: Evaluation of the Warm-Season Diurnal  
Variability over East Asia in Recent Reanalyses JRA-55, ERA-Interim, NCEP CFSR, and  
NASA MERRA, *Journal of Climate*, 27, 5517-5537,  
<https://doi.org/10.1175/JCLI-D-14-00005.1>, 2014.
- 580 Dee, D. P., Uppala, S. M., Simmons, A. J., Berrisford, P., Poli, P., Kobayashi, S., Andrae, U.,  
Balmaseda, M. A., Balsamo, G., Bauer, P., Bechtold, P., Beljaars, A. C. M., van de Berg,  
L., Bidlot, J., Bormann, N., Delsol, C., Dragani, R., Fuentes, M., Geer, A. J., Haimberger,  
L., Healy, S. B., Hersbach, H., Hólm, E. V., Isaksen, L., Kållberg, P., Köhler, M.,  
Matricardi, M., McNally, A. P., Monge-Sanz, B. M., Morcrette, J. J., Park, B. K., Peubey,  
C., de Rosnay, P., Tavolato, C., Thépaut, J. N., and Vitart, F.: The ERA-Interim reanalysis:  
585 configuration and performance of the data assimilation system, *Quarterly Journal of the  
Royal Meteorological Society*, 137, 553-597, <https://doi.org/10.1002/qj.828>, 2011.
- 590 Fukui, S., Iwasaki, T., Saito, K., Seko, H., and Kunii, M.: A Feasibility Study on the  
High-Resolution Regional Reanalysis over Japan Assimilating Only Conventional  
Observations as an Alternative to the Dynamical Downscaling, *Journal of the  
Meteorological Society of Japan. Ser. II*, 96, 565-585,  
<https://doi.org/10.2151/jmsj.2018-056>, 2018.
- Gao, S., Huang, D., Du, N., Ren, C., and Yu, H.: WRF ensemble dynamical downscaling of  
precipitation over China using different cumulus convective schemes, *Atmospheric  
Research*, 271, 106116, <https://doi.org/10.1016/j.atmosres.2022.106116>, 2022.
- 595 Gelaro, R., McCarty, W., Suárez, M. J., Todling, R., Molod, A., Takacs, L., Randles, C. A.,  
Darmenov, A., Bosilovich, M. G., Reichle, R., Wargan, K., Coy, L., Cullather, R., Draper,  
C., Akella, S., Buchard, V., Conaty, A., da Silva, A. M., Gu, W., Kim, G.-K., Koster, R.,  
Lucchesi, R., Merkova, D., Nielsen, J. E., Partyka, G., Pawson, S., Putman, W., Rienecker,

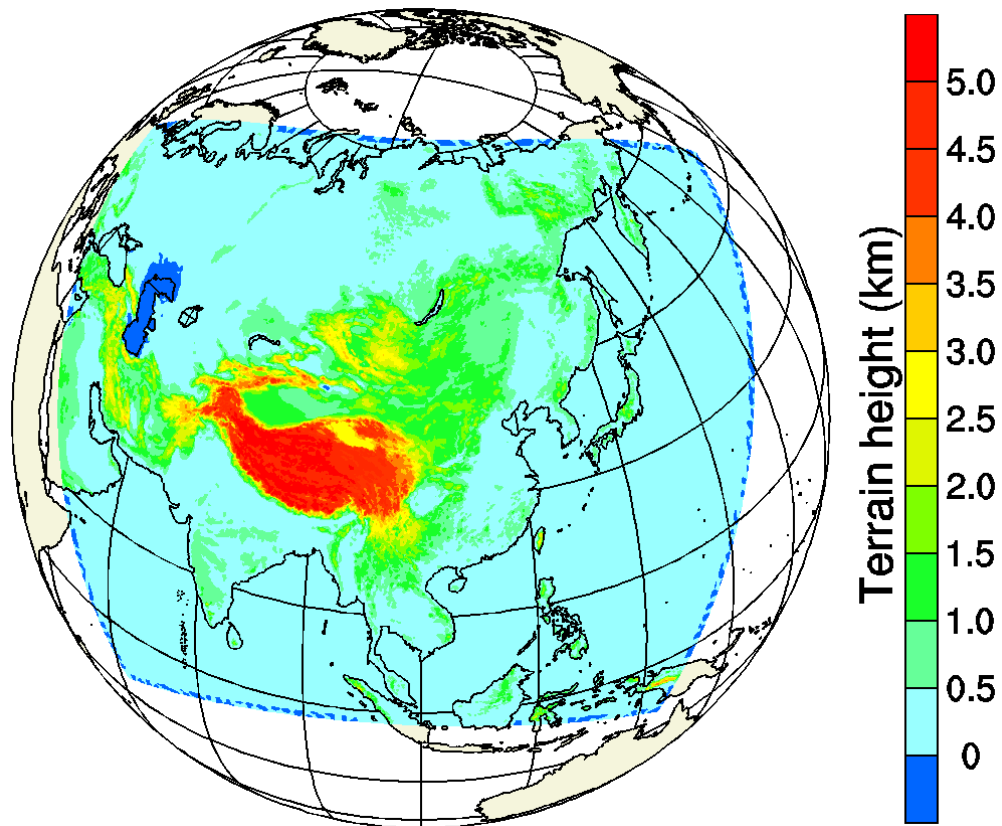
- M., Schubert, S. D., Sienkiewicz, M., and Zhao, B.: The Modern-Era Retrospective Analysis for Research and Applications, Version 2 (MERRA-2), *Journal of Climate*, 30, 5419-5454, <https://doi.org/10.1175/JCLI-D-16-0758.1>, 2017.
- 600 Gong, Y., Yang, S., Yin, J., Wang, S., Pan, X., Li, D., and Yi, X.: Validation of the Reproducibility of Warm-Season Northeast China Cold Vortices for ERA5 and MERRA-2 Reanalysis, *Journal of Applied Meteorology and Climatology*, 61, 1349-1366, <https://doi.org/10.1175/JAMC-D-22-0052.1>, 2022.
- 605 Hersbach, H., Bell, B., Berrisford, P., Hirahara, S., Horányi, A., Muñoz-Sabater, J., Nicolas, J., Peubey, C., Radu, R., Schepers, D., Simmons, A., Soci, C., Abdalla, S., Abellan, X., Balsamo, G., Bechtold, P., Biavati, G., Bidlot, J., Bonavita, M., De Chiara, G., Dahlgren, P., Dee, D., Diamantakis, M., Dragani, R., Flemming, J., Forbes, R., Fuentes, M., Geer, A., Haimberger, L., Healy, S., Hogan, R. J., Hólm, E., Janisková, M., Keeley, S., Laloyaux, P., Lopez, P., Lupu, C., Radnoti, G., de Rosnay, P., Rozum, I., Vamborg, F., Villaume, S., and Thépaut, J.-N.: The ERA5 global reanalysis, *Quarterly Journal of the Royal Meteorological Society*, 146, 1999-2049, <https://doi.org/10.1002/qj.3803>, 2020.
- 610 Hong, S.-Y., Noh, Y., and Dudhia, J.: A new vertical diffusion package with an explicit treatment of entrainment processes, *Monthly Weather Review*, 134, 2318-2341, <https://doi.org/10.1175/MWR3199.1>, 2006.
- 615 Hu, M., Ge, G., Zhou, C., Stark, D., Shao, H., Newman, K., Beck, J., and Zhang, X.: Grid-point Statistical Interpolation (GSI) User's Guide Version 3.7. Developmental Testbed Center. Available at <https://dtcenter.org/community-code/gridpoint-statistical-interpolation-gsi/documentation> (last access 10 January 2023), 149 pp, 2018.
- 620 Hu, M. and Xue, M.: Implementation and evaluation of cloud analysis with WSR-88D reflectivity data for GSI and WRF-ARW, *Geophysical Research Letters*, 34, <https://doi.org/10.1029/2006GL028847>, 2007.
- 625 Huang, J., Yin, J., Wang, M., He, Q., Guo, J., Zhang, J., Liang, X., and Xie, Y.: Evaluation of Five Reanalysis Products With Radiosonde Observations Over the Central Taklimakan Desert During Summer, *Earth and Space Science*, 8, e2021EA001707, <https://doi.org/10.1029/2021EA001707>, 2021.
- 630 Iacono, M. J., Delamere, J. S., Mlawer, E. J., Shephard, M. W., Clough, S. A., and Collins, W. D.: Radiative forcing by long-lived greenhouse gases: Calculations with the AER radiative transfer models, *Journal of Geophysical Research: Atmospheres*, 113, <https://doi.org/10.1029/2008JD009944>, 2008.
- 635 Ingleby, B., Pauley, P., Kats, A., Ator, J., Keyser, D., Doerenbecher, A., Fucile, E., Hasegawa, J., Toyoda, E., Kleinert, T., Qu, W., St. James, J., Tennant, W., and Weedon, R.: Progress toward High-Resolution, Real-Time Radiosonde Reports, *Bulletin of the American Meteorological Society*, 97, 2149-2161, <https://doi.org/10.1175/BAMS-D-15-00169.1>, 2016.
- Jakob, D., Su, C.-H., Eizenberg, N., Kociuba, G., Steinle, P., Fox-Hughes, P., and Bettio, L.: An atmospheric high-resolution regional reanalysis for Australia, *The Bulletin of the Australian Meteorological and Oceanographic Society*, 30, 16-23, 2017.
- 640 James, E. P., Benjamin, S. G., and Jamison, B. D.: Commercial-Aircraft-Based Observations for NWP: Global Coverage, Data Impacts, and COVID-19, *Journal of Applied Meteorology and Climatology*, 59, 1809-1825, <https://doi.org/10.1175/JAMC-D-20-0010.1>, 2020.
- 645 Janjić, Z. I.: The step-mountain eta coordinate model: further developments of the convection, viscous sublayer, and turbulence closure schemes, *Monthly Weather Review*, 122, 927-945, [https://doi.org/10.1175/1520-0493\(1994\)122<0927:TSMECM>2.0.CO;2](https://doi.org/10.1175/1520-0493(1994)122<0927:TSMECM>2.0.CO;2), 1994.
- Jiang, H., Xu, W., Yang, S., Zhu, Y., Zhou, Z., and Liao, J.: Development of an Integrated

- Global Land Surface Dataset from 1901 to 2018, *Journal of Meteorological Research*, 35, 789-798, <https://doi.org/10.1007/s13351-021-1058-2>, 2021.
- 650 Kain, J. S.: The Kain–Fritsch Convective Parameterization: An Update, *Journal of Applied Meteorology*, 43, 170-181, [https://doi.org/10.1175/1520-0450\(2004\)043<0170:TKCPAU>2.0.CO;2](https://doi.org/10.1175/1520-0450(2004)043<0170:TKCPAU>2.0.CO;2), 2004.
- Kanamitsu, M., Ebisuzaki, W., Woollen, J., Yang, S.-K., Hnilo, J. J., Fiorino, M., and Potter, G. L.: NCEP–DOE AMIP-II Reanalysis (R-2), *Bulletin of the American Meteorological Society*, 83, 1631-1644, <https://doi.org/10.1175/BAMS-83-11-1631>, 2002.
- 655 Kawai, Y., Moteki, Q., Kuwano-Yoshida, A., Enomoto, T., Manda, A., and Nakamura, H.: Impact Propagation of Radiosonde Data Assimilation over the Kuroshio and Kuroshio Extension: Case Study on the Early Summer (Baiu) in 2012, *Journal of the Meteorological Society of Japan. Ser. II*, 95, 71-90, <https://doi.org/10.2151/jmsj.2017-004>, 2017.
- 660 Kobayashi, S., Ota, Y., Harada, Y., Ebata, A., Moriya, M., Onoda, H., Onogi, K., Kamahori, H., Kobayashi, C., Endo, H., Miyaoka, K., and Takahashi, K.: The JRA-55 Reanalysis: General Specifications and Basic Characteristics, *Journal of the Meteorological Society of Japan. Ser. II*, 93, 5-48, <https://doi.org/10.2151/jmsj.2015-001>, 2015.
- 665 Lee, M.-H., Kim, J.-H., Song, H.-J., Inoue, J., Sato, K., and Yamazaki, A.: Potential benefit of extra radiosonde observations around the Chukchi Sea for the Alaskan short-range weather forecast, *Polar Science*, 21, 124-135, <https://doi.org/10.1016/j.polar.2018.12.005>, 2019.
- Li, J., Chen, T., and Li, N.: Diurnal Variation of Summer Precipitation across the Central Tian Shan Mountains, *Journal of Applied Meteorology and Climatology*, 56, 1537-1550, <https://doi.org/10.1175/JAMC-D-16-0265.1>, 2017.
- 670 Li, Y., Wang, D., and Yin, J.: Evaluations of different boundary layer schemes on low-level wind prediction in western Inner Mongolia, *Acta Scientiarum Naturalium Universitatis Sunyatseni*, 57, 17-29, <https://doi.org/10.13471/j.cnki.acta.snus.2018.04.0032018>.
- Liang, X., Yin, J., Xie, Y., and Li, F.: East Asia Reanalysis System of CMA, EGU General Assembly 2020, Online, 4–8 May 2020, EGU2020-1914, <https://doi.org/10.5194/egusphere-egu2020-1914>,
- 675 <https://doi.org/10.5194/egusphere-egu2020-1914>,
- Liang, X., Xie, Y., Yin, J., Luo, Y., Yao, D., and Li, F.: An IVAP-based dealiasing method for radar velocity data quality control, *Journal of Atmospheric and Oceanic Technology*, <https://doi.org/10.1175/JTECH-D-18-0216.1>, 2019.
- 680 Liao, J., Wang, H., Zhou, Z., Liu, Z., Jiang, L., and Yuan, F.: Integration, Quality Assurance, and Usage of Global Aircraft Observations in CRA, *Journal of Meteorological Research*, 35, 1-16, <https://doi.org/10.1007/s13351-021-0093-3>, 2021.
- Luo, Y., Zhang, R., Wan, Q., Wang, B., Wong, W. K., Hu, Z., Jou, B. J.-D., Lin, Y., Johnson, R. H., Chang, C.-P., Zhu, Y., Zhang, X., Wang, H., Xia, R., Ma, J., Zhang, D.-L., Gao, M., Zhang, Y., Liu, X., Chen, Y., Huang, H., Bao, X., Ruan, Z., Cui, Z., Meng, Z., Sun, J., Wu, M., Wang, H., Peng, X., Qian, W., Zhao, K., and Xiao, Y.: The Southern China Monsoon Rainfall Experiment (SCMREX), *Bulletin of the American Meteorological Society*, 98, 999-1013, <https://doi.org/10.1175/BAMS-D-15-00235.1>, 2017.
- 685 Mahmood, S., Davie, J., Jerney, P., Renshaw, R., George, J. P., Rajagopal, E. N., and Rani, S. I.: Indian monsoon data assimilation and analysis regional reanalysis: Configuration and performance, *Atmospheric Science Letters*, 19, e808, <https://doi.org/10.1002/asl.808>, 2018.
- 690 Mao, J., Shi, X., Ma, L., Kaiser, D. P., Li, Q., and Thornton, P. E.: Assessment of Reanalysis Daily Extreme Temperatures with China’s Homogenized Historical Dataset during 1979–2001 Using Probability Density Functions, *Journal of Climate*, 23, 6605-6623, <https://doi.org/10.1175/2010JCLI3581.1>, 2010.
- 695 Mesinger, F., DiMego, G., Kalnay, E., Mitchell, K., Shafran, P. C., Ebisuzaki, W., Jović, D.,

- 700 Woollen, J., Rogers, E., Berbery, E. H., Ek, M. B., Fan, Y., Grumbine, R., Higgins, W., Li, H., Lin, Y., Manikin, G., Parrish, D., and Shi, W.: North American Regional Reanalysis, *Bulletin of the American Meteorological Society*, 87, 343-360, <https://doi.org/10.1175/BAMS-87-3-343>, 2006.
- 705 Mirza, A. K., Ballard, S. P., Dance, S. L., Maisey, P., Rooney, G. G., and Stone, E. K.: Comparison of aircraft-derived observations with in situ research aircraft measurements, *Quarterly Journal of the Royal Meteorological Society*, 142, 2949-2967, <https://doi.org/10.1002/qj.2864>, 2016.
- 710 Newman, K., Opatz, J., Jensen, T., Prestopnik, J., Soh, H., Goodrich, L., Brown, B., Bullock, R., and Gotway, J. H.: The MET Version 10.1.2 User's Guide Developmental Testbed Center. Available at: <https://github.com/dtcenter/MET/releases> (last access 2 Oct 2022), Developmental Testbed Center. Available at: <https://github.com/dtcenter/MET/releases>, 2022.
- 715 Niu, G.-Y., Yang, Z.-L., Mitchell, K. E., Chen, F., Ek, M. B., Barlage, M., Kumar, A., Manning, K., Niyogi, D., Rosero, E., Tewari, M., and Xia, Y.: The community Noah land surface model with multiparameterization options (Noah-MP): 1. Model description and evaluation with local-scale measurements, *Journal of Geophysical Research: Atmospheres*, 116, D12109, <https://doi.org/10.1029/2010JD015139>, 2011.
- Qiu, Y., Hu, Q., and Zhang, C.: WRF simulation and downscaling of local climate in Central Asia, *International Journal of Climatology*, 37, 513-528, <https://doi.org/10.1002/joc.5018>, 2017.
- 720 Rabier, F., Faccani, C., Fourrié, N., Agusti-Panareda, A., Karbou, F., Moll, P., Lafore, J. P., Nuret, M., Hdidou, F., and Bock, O.: The Impacts of AMMA Radiosonde Data on the French Global Assimilation and Forecast System, *Weather and Forecasting*, 24, <https://doi.org/10.1175/2009WAF2222237.1>, 2009.
- Reen, B.: A brief guide to observation nudging in WRF, [www2.mmm.ucar.edu/wrf/users/docs/ObsNudgingGuide.pdf](http://www2.mmm.ucar.edu/wrf/users/docs/ObsNudgingGuide.pdf), 2016.
- 725 Skamarock, W., Klemp, J., Dudhia, J., Gill, D., Barker, D., Duda, M., Huang, X.-Y., Wang, W., and Powers, J.: A Description of the Advanced Research WRF Version 3. NCAR Tech. Note NCAR/TN-475+STR, 10.13140/RG.2.1.2310.6645, 2008.
- Thompson, G., Field, P. R., Rasmussen, R. M., and Hall, W. D.: Explicit forecasts of winter precipitation using an improved bulk microphysics scheme. Part II: Implementation of a new snow parameterization, *Monthly Weather Review*, 136, 5095-5115, <https://doi.org/10.1175/2008MWR2387.1>, 2008.
- 730 Usui, N., Wakamatsu, T., Tanaka, Y., Hirose, N., Toyoda, T., Nishikawa, S., Fujii, Y., Takatsuki, Y., Igarashi, H., Nishikawa, H., Ishikawa, Y., Kuragano, T., and Kamachi, M.: Four-dimensional variational ocean reanalysis: a 30-year high-resolution dataset in the western North Pacific (FORA-WNP30), *Journal of Oceanography*, 73, 205-233, <https://doi.org/10.1007/s10872-016-0398-5>, 2017.
- Vidal, J.-P., Martin, E., Franchistéguy, L., Baillon, M., and Soubeyroux, J.-M.: A 50-year high-resolution atmospheric reanalysis over France with the Safran system, *International Journal of Climatology*, 30, 1627-1644, <https://doi.org/10.1002/joc.2003>, 2010.
- 740 Wang, W., Bruyère, C., Duda, M., and Dudhia, J.: User's Guides for the Advanced Research WRF (ARW) Modeling System, [http://www2.mmm.ucar.edu/wrf/users/docs/user\\_guide\\_V3/contents.html](http://www2.mmm.ucar.edu/wrf/users/docs/user_guide_V3/contents.html), 2017.
- Wright, J. S., Fujiwara, M., and Long, C.: Description of the Reanalysis Systems, in: the SPARC Reanalysis Intercomparison Project (S-RIP), <https://jonathonwright.github.io/>, 138 pp, <https://jonathonwright.github.io/>, <https://jonathonwright.github.io/>, 2019.
- 745 Wu, W., Zou, H., Shan, J., and Wu, S.: A Dynamical Z-R Relationship for Precipitation Estimation Based on Radar Echo-Top Height Classification, *Advances in Meteorology*,

- 2018, 11, <https://doi.org/10.1155/2018/8202031>, 2018.
- 750 Yang, E. G., Kim, H. M., and Kim, D. H.: Development of East Asia Regional Reanalysis based on advanced hybrid gain data assimilation method and evaluation with E3DVAR, ERA-5, and ERA-Interim reanalysis, *Earth Syst. Sci. Data*, 14, 2109-2127, <https://doi.org/10.5194/essd-14-2109-2022>, 2022.
- 755 Yang, L., Liang, X., Yin, J., Xie, Y., and Fan, H.: Evaluation of the Precipitation of the East Asia regional reanalysis system mainly over mainland China, *International Journal of Climatology*, <https://doi.org/10.1002/joc.7940>, 2023.
- Yin, J., Wang, D., and Zhai, G.: A study of characteristics of the cloud microphysical parameterization schemes in mesoscale models and its applicability to China, *Advances in Earth Science*, 29, 238-249, <https://doi.org/10.11867/J.ISSN.1001-8166.2014.02-0238>, 2014.
- 760 Yin, J., Gu, H., Huang, J., and Wang, M.: An investigation into the vertical structures of low-altitude atmosphere over the Central Taklimakan Desert in summer, *Atmospheric Science Letters*, e01042, <https://doi.org/10.1002/asl.1042>, 2021.
- Yin, J., Liang, X., Xie, Y., and Chen, F.: Development of East Asia Reanalysis System (EARS), American Geophysical Union, Fall Meeting 2019, abstract #A24I-08, 2019
- 765 Yin, J., Liang, X., Chen, F., Liu, Y., He, H., Liang, Z., Zou, H., Xu, J., Hao, S., and Xie, Y.: Development of atmospheric data assimilation techniques and regional reanalysis datasets in the East Asia, *Advances in Meteorological Science and Technology*, 8, 79-84, <https://doi.org/10.3969/j.issn.2095-1973.2018.01.009>, 2018.
- 770 Yin, J., Liang, X., Xie, Y., Li, F., Hu, K., Cao, L., Chen, F., Zou, H., Zhu, F., Sun, X., Xu, J., Wang, G., Zhao, Y., and Liu, J.: East Asia Reanalysis System (EARS) [Data set], Zenodo, <https://doi.org/10.5281/zenodo.7404918>, 2022.
- Yin, J., Zhang, D.-L., Luo, Y., and Ma, R.: On the Extreme Rainfall Event of 7 May 2017 Over the Coastal City of Guangzhou. Part I: Impacts of Urbanization and Orography, *Monthly Weather Review*, 148, 955-979, 10.1175/MWR-D-19-0212.1, 2020.
- 775 Zhang, G., Xue, H., Xu, J., Chen, J., and He, H.: The WRF performance comparison based on Noah and Noah-MP land surface processes on East Asia, *Meteorological Monthly*, 42, 1058-1068, <https://doi.org/10.7519/j.issn.1000-0526.2016.09.003>, 2016.
- Zhang, J., Zhao, T., Li, Z., Li, C., Li, Z., Ying, K., Shi, C., Jiang, L., and Zhang, W.: Evaluation of Surface Relative Humidity in China from the CRA-40 and Current Reanalyses, *Adv. Atmos. Sci.*, 38, 1958-1976, <https://doi.org/10.1007/s00376-021-0333-6>, 2021.
- 780 Zhao, S., W. He, and Y. Jiang, 2018: Evaluation of NCEP-2 and CFSR reanalysis seasonal temperature data in China using detrended fluctuation analysis. *International Journal of Climatology*, 38, 252-263, <https://doi.org/10.1002/joc.5173>.
- 785 Zhao, P., Xu, X., Chen, F., Guo, X., Zheng, X., Liu, L., Hong, Y., Li, Y., La, Z., Peng, H., Zhong, L., Ma, Y., Tang, S., Liu, Y., Liu, H., Li, Y., Zhang, Q., Hu, Z., Sun, J., Zhang, S., Dong, L., Zhang, H., Zhao, Y., Yan, X., Xiao, A., Wan, W., Liu, Y., Chen, J., Liu, G., Zhaxi, Y., and Zhou, X.: The Third Atmospheric Scientific Experiment for Understanding the Earth–Atmosphere Coupled System over the Tibetan Plateau and Its Effects, *Bulletin of the American Meteorological Society*, 99, 757-776, <https://doi.org/10.1175/BAMS-D-16-0050.1>, 2018.
- 790 Zou, H., Shan, J., and Deng, S.: Study of the doppler radar data gridding, *Meteorology and Disaster Reduction Research*, 37, 23-30, 2014.
- 795 Zou, H., Zhang, S., Liang, X., and Yi, X.: Improved algorithms for removing isolated non-meteorological echoes and ground clutters in CINRAD, *Journal of Meteorological Research*, 32, 584-597, <https://doi.org/10.1007/s13351-018-7176-9>, 2018.

## Figures



800 **Fig. 1** The East Asia Reanalysis System (EARS) domain in the WRF model, and its 12-km topography. The shading indicates the height of the terrain in the model.

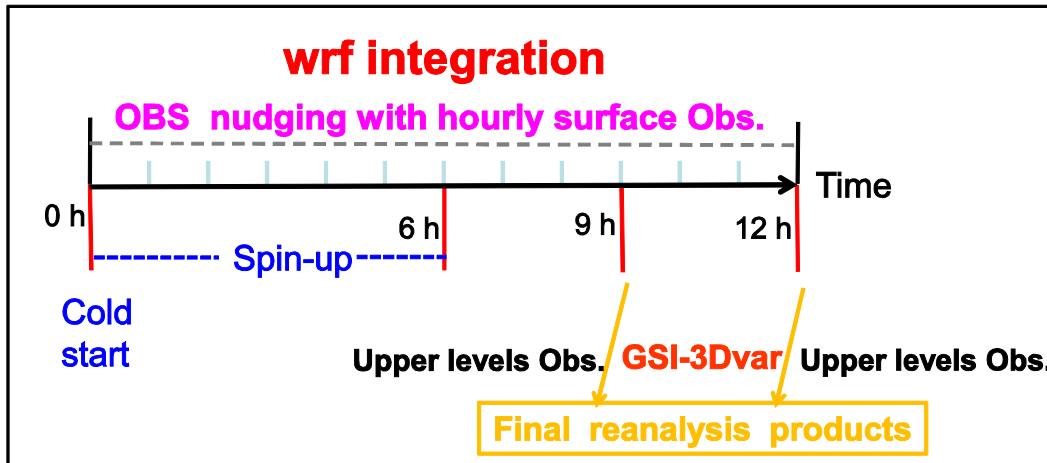


**Fig. 2** Schematic illustrating the flow chart of analysis steps of the EARS. See text for details.

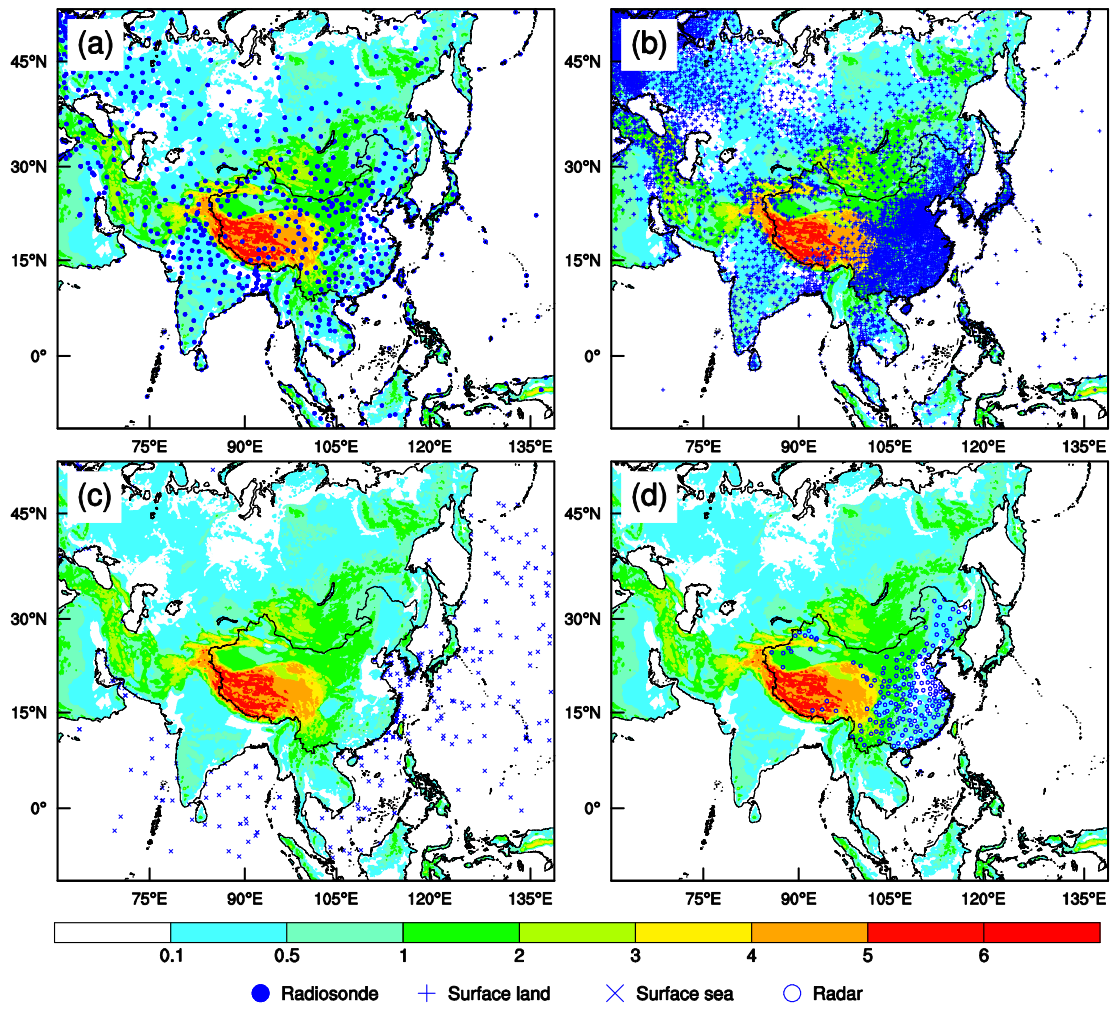


**Fig. 3** Spatial distributions of (a) radiosonde, (b) land, (c) sea, and (d) radar observations for EARS.



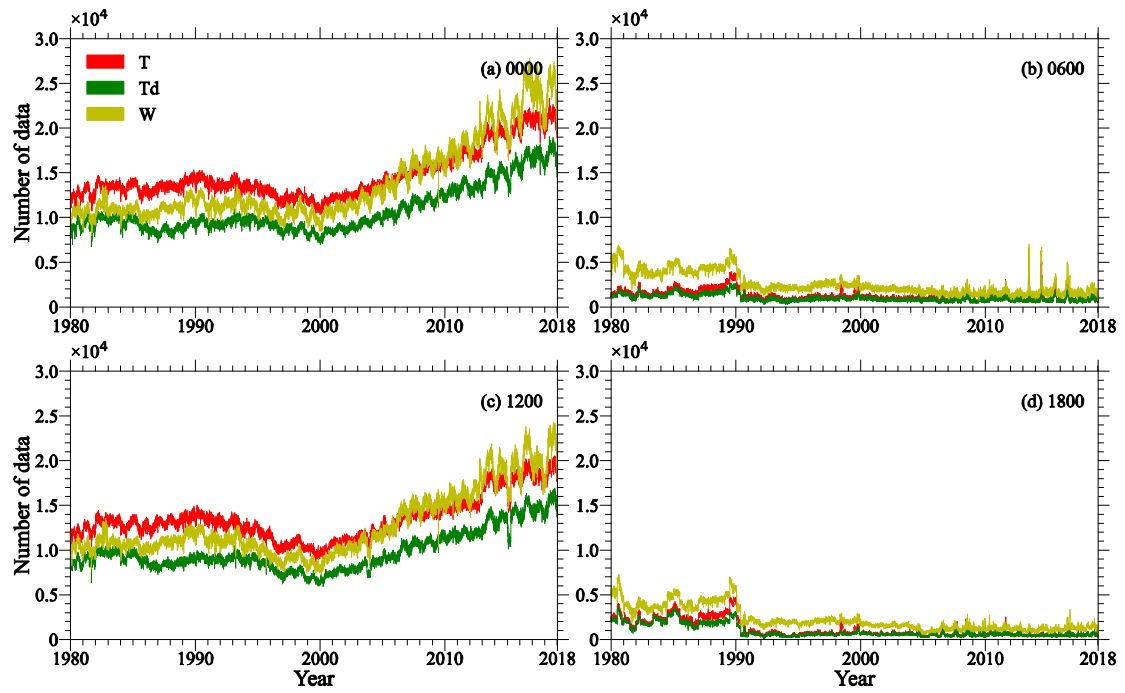
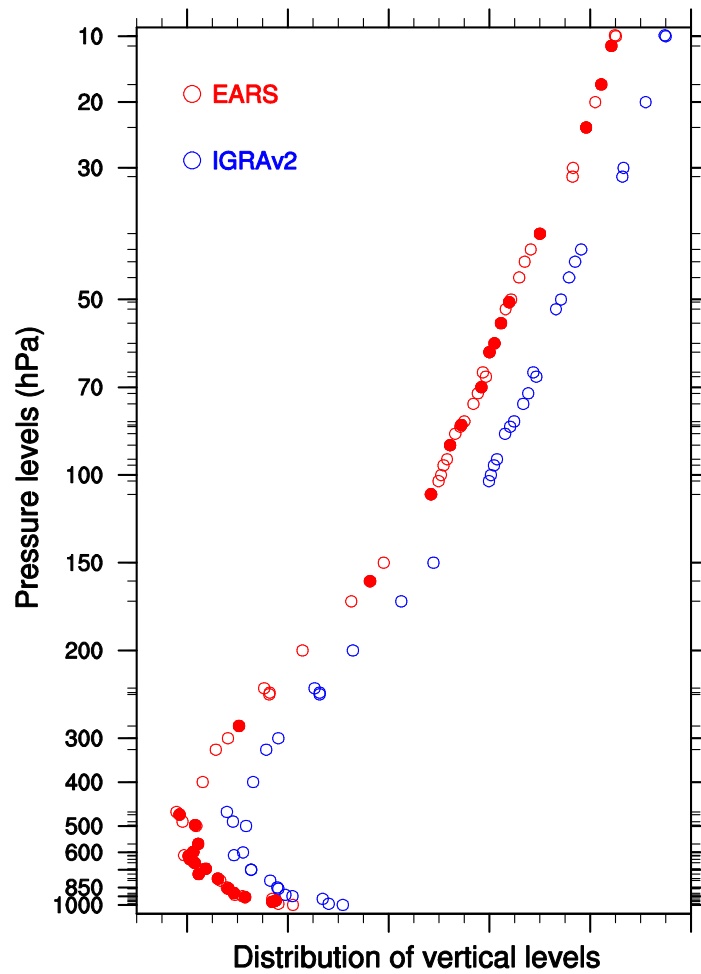
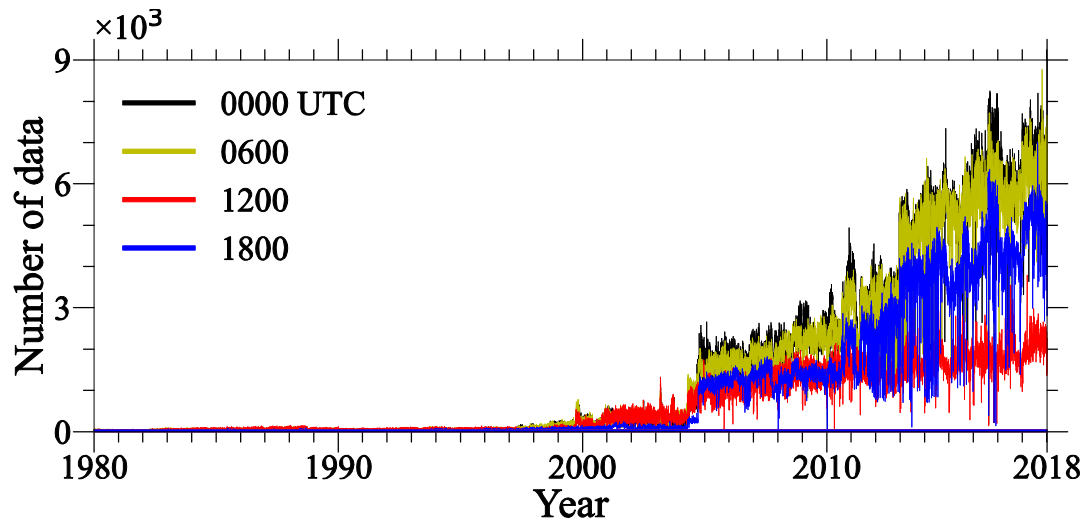


**Fig. 4** Counts of radiosonde observations assimilated in EARS at (a) 0000, (b) 0600, (c) 1200, and (d) 1800 UTC.  $T$ ,  $T_d$ , and  $W$  denote temperature, dew-temperature, and horizontal wind, respectively.



815 **Fig. 5** Comparison of merged radiosonde (red) used in EARS and the Integrated Global Radiosonde Archive version 2 (IGRAv2, blue) at Beijing station (54511) at 0000 UTC 1 July 2016. The red dots represent the newly-merged from paper-based records that have never been used in any atmospheric reanalysis system outside of China. Note that the IGRaV2 profile was shifted to the left to avoid overlaying the two datasets. The two profiles are perfectly overlapped except for newly added observation points.



820

**Fig. 6** Counts of aircraft observations used in EARS at 0000, 0600, 1200, and 1800 UTC.

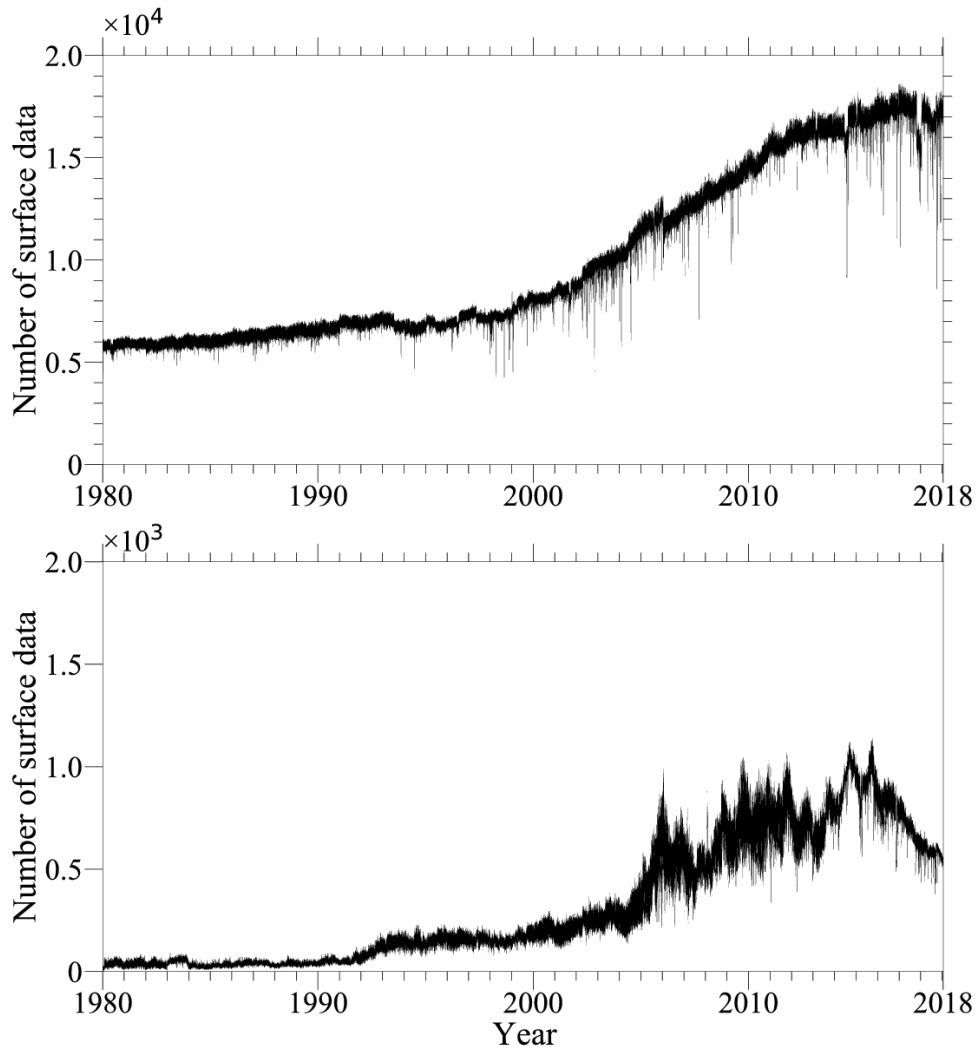
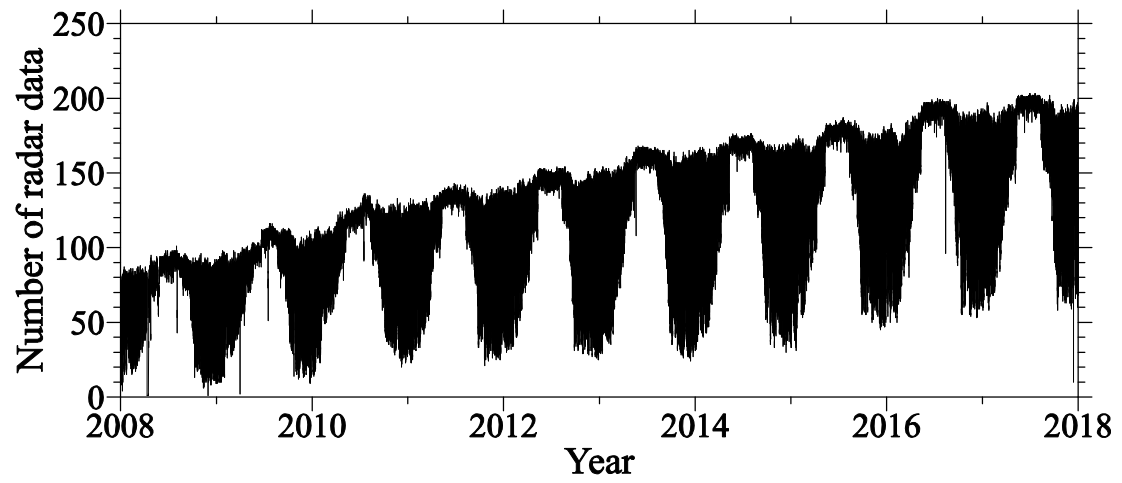


**Fig. 7** Counts of the surface observations over (a) land and (b) sea used in EARS.



825

**Fig. 8** Counts of the ground-based radar stations used in EARS.

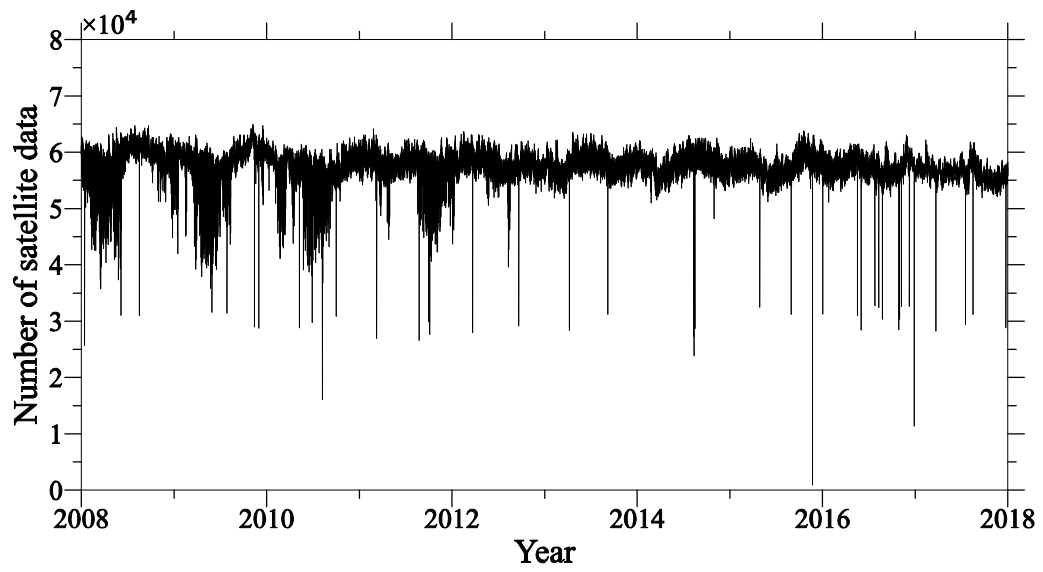
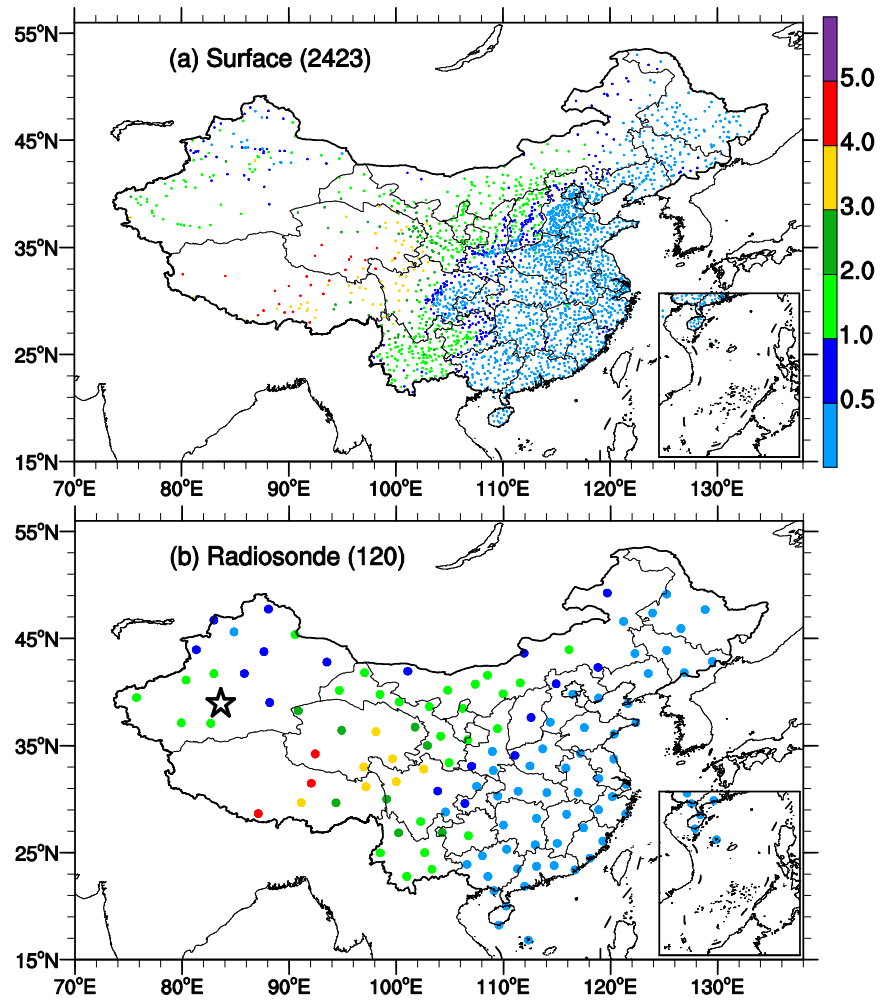
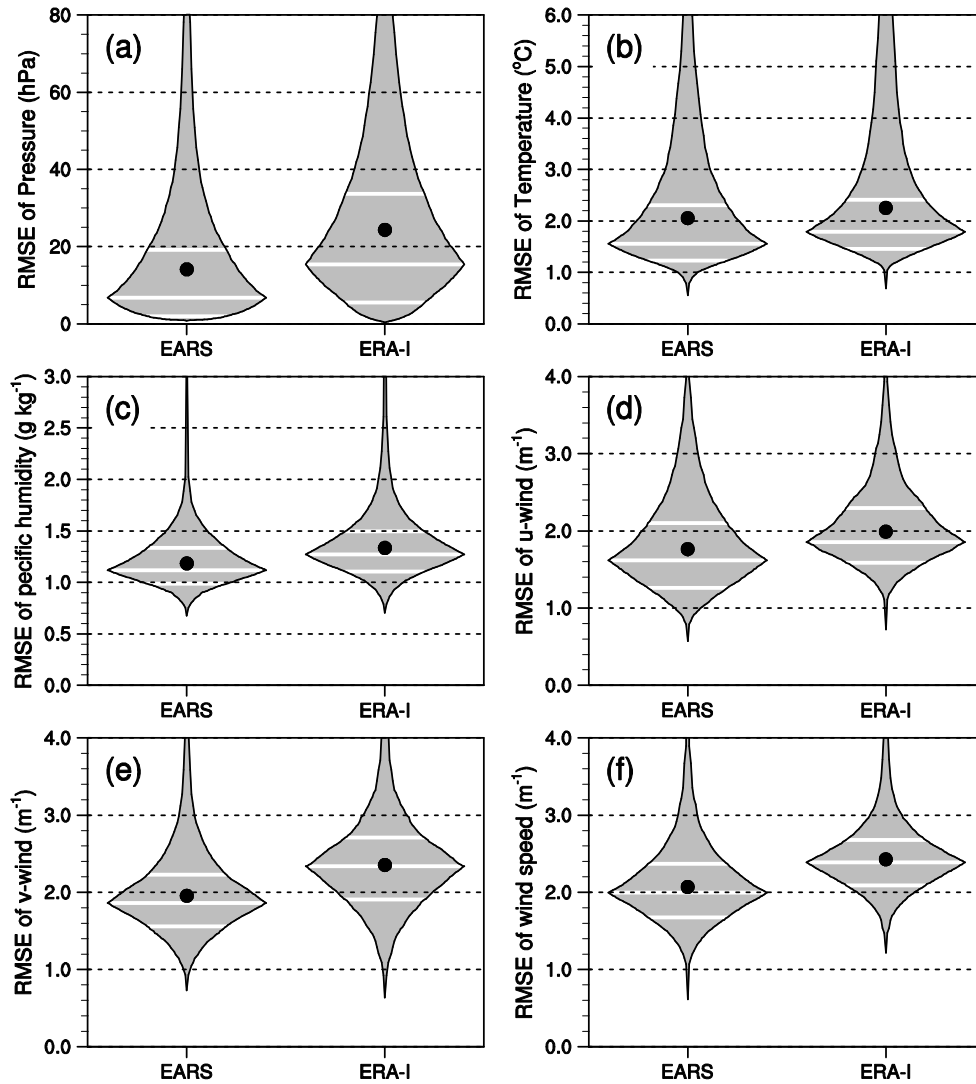


**Fig. 9** Counts of cloud-derived wind vectors from the Fengyun-2 (FY-2) geostationary meteorological satellite observations, which are used in the EARS.



830

**Fig. 10** Spatial distributions of selected (a) surface and (b) radiosonde stations for verification. The number in parenthesis is the observational count. The color of the dot indicates terrain (km). In (b), the star denotes the location of a radiosonde observational field experiment at the central Taklimakan Desert, China.



835

**Fig. 11** Comparison of averaged root mean square error (RMSE) between EARS and ERA-Interim in terms of surface meteorological variables: (a) pressure ( $P$ ; hPa), (b) temperature ( $T$ ;  $^{\circ}\text{C}$ ), (c) specific humidity ( $Q$ ;  $\text{g kg}^{-1}$ ), (d) zonal wind ( $U$ ;  $\text{m s}^{-1}$ ), (e) meridional wind ( $V$ ;  $\text{m s}^{-1}$ ), and (f) wind speed ( $WS$ ;  $\text{m s}^{-1}$ ). The black dot denotes the averaged value of each category; and the horizontal white lines indicate the 25th, 50th (median), and 75th percentiles. See text for details.

840



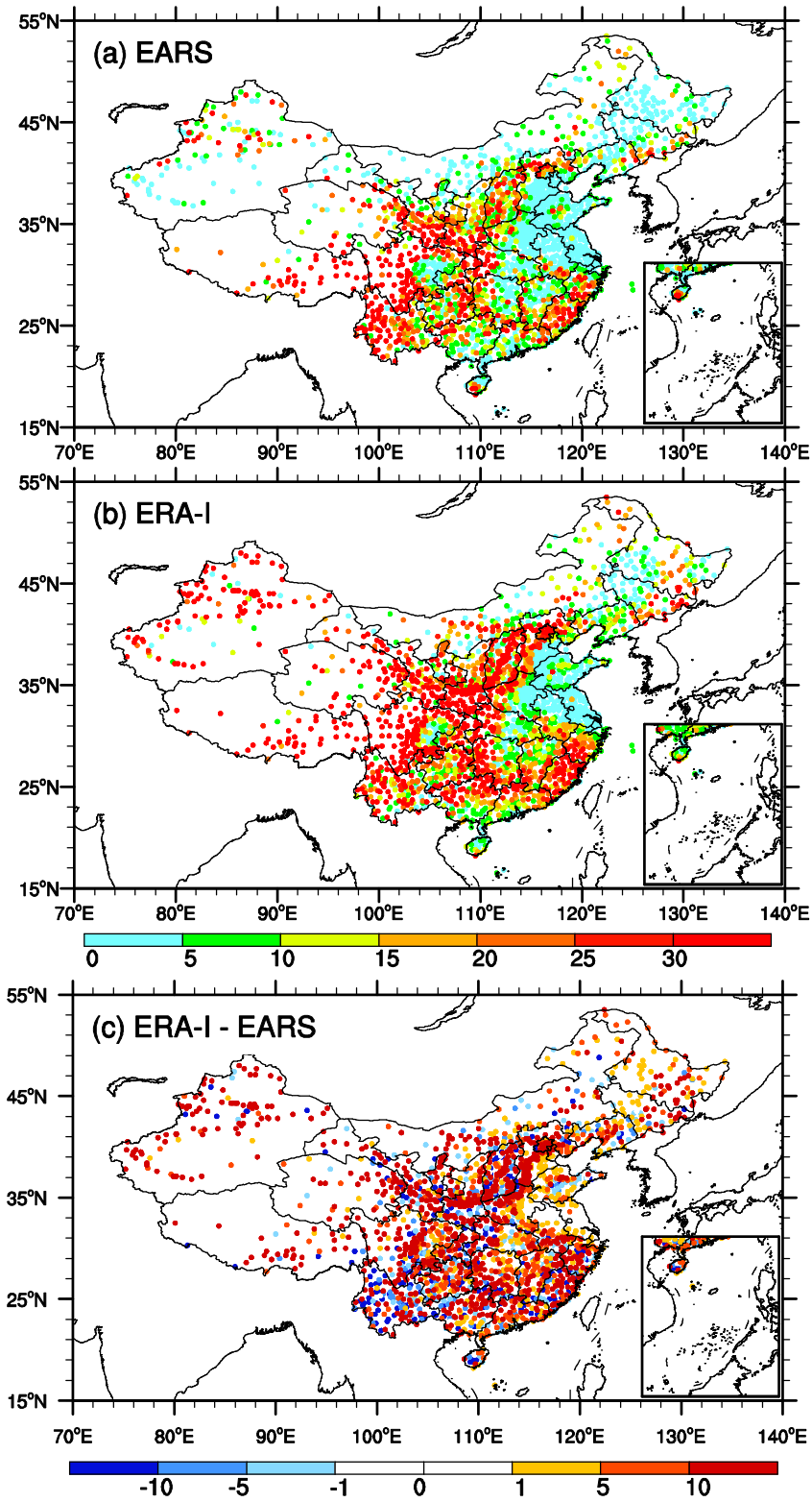
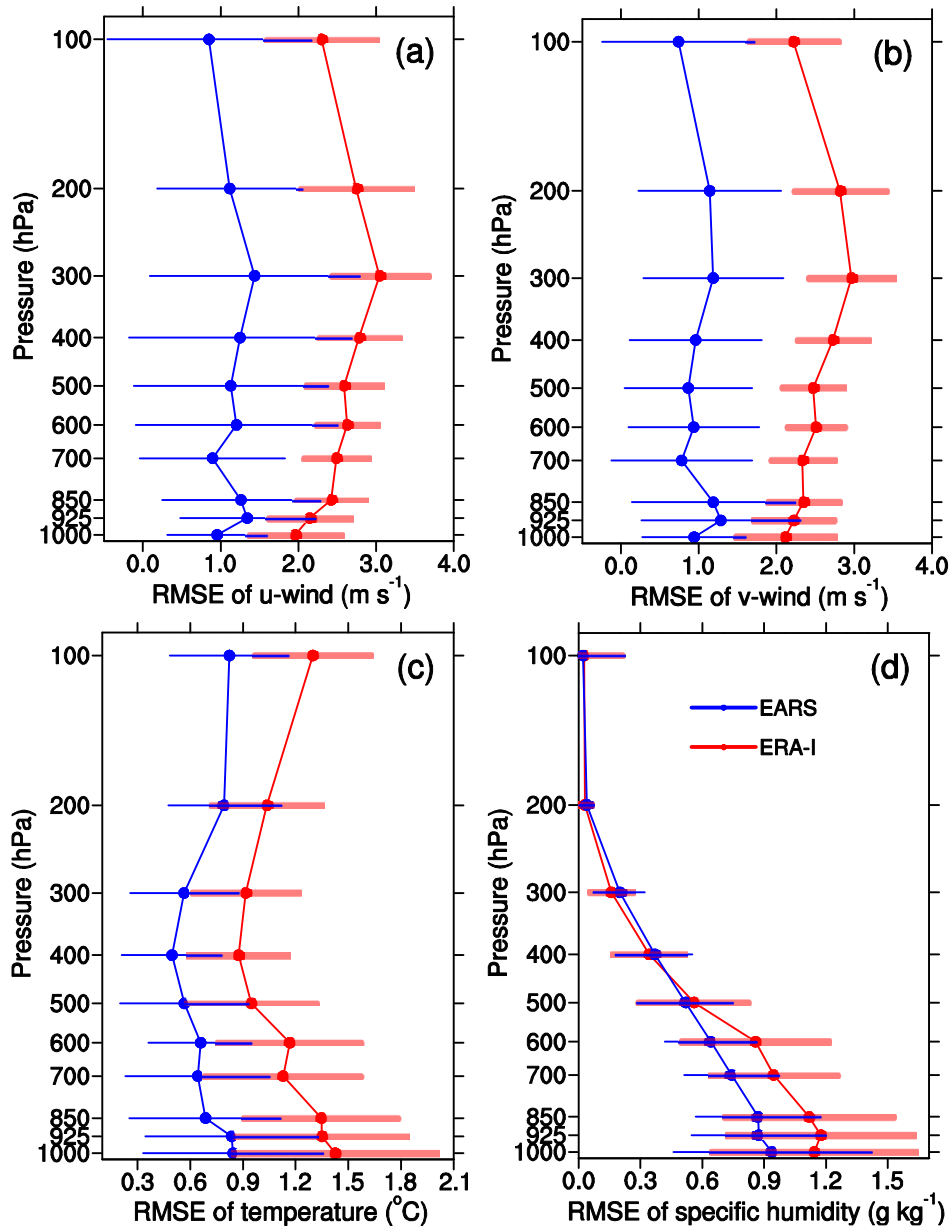
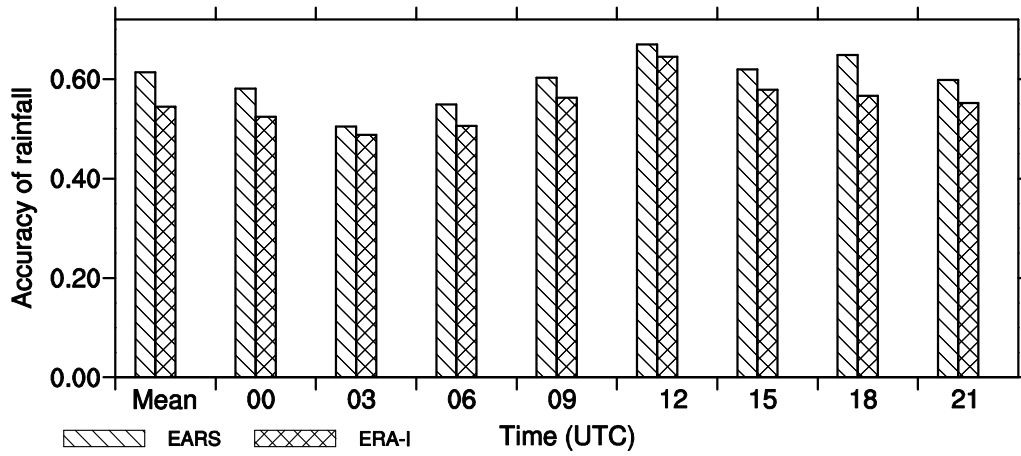


**Fig. 12** Spatial distributions of averaged RMSE of surface pressure ( $P$ ; hPa) from (a) EARS and (b) ERA-Interim; and (c) their differences (ERA-I minus EARS).



845

**Fig. 13** Comparison of averaged RMSEs of EARS (blue) and ERA-Interim (red) at different levels for (a) u-wind ( $U$ ;  $m s^{-1}$ ), (b) v-wind ( $V$ ;  $m s^{-1}$ ), (c) temperature ( $T$ ;  $^{\circ}C$ ), and (d) specific humidity ( $Q$ ;  $g kg^{-1}$ ). Standard deviation of RMSE at each level is marked.



850

**Fig. 14** Comparison of the accuracy of 3-h accumulated rainfall between EARS and ERA-Interim in different episodes. Mean denotes the averaged value for all times.

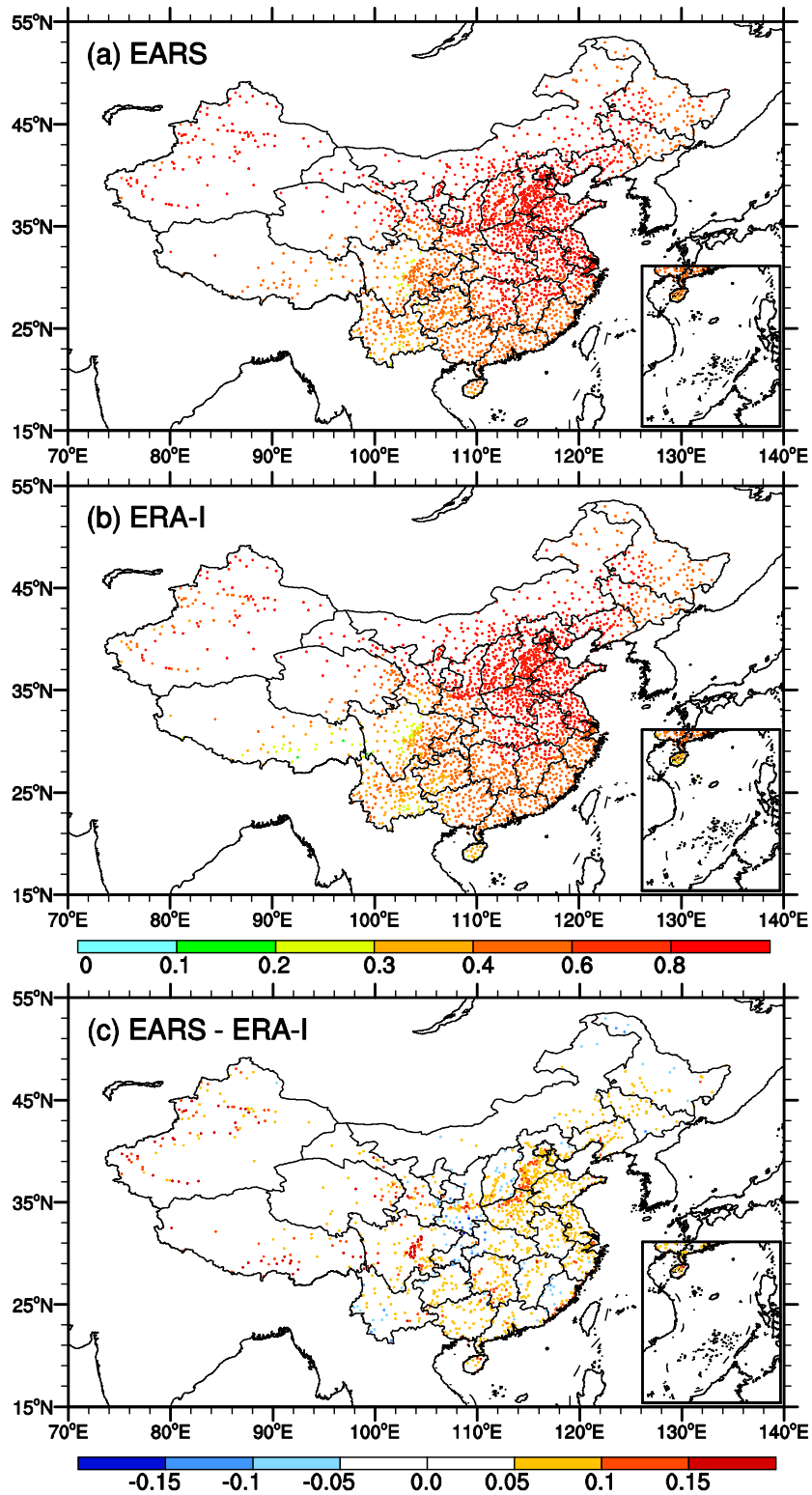


**Fig. 15** Spatial distributions of averaged rainfall accuracy of (a) EARS, (b) ERA-Interim, and their difference (EARS minus ERA-I).  
855

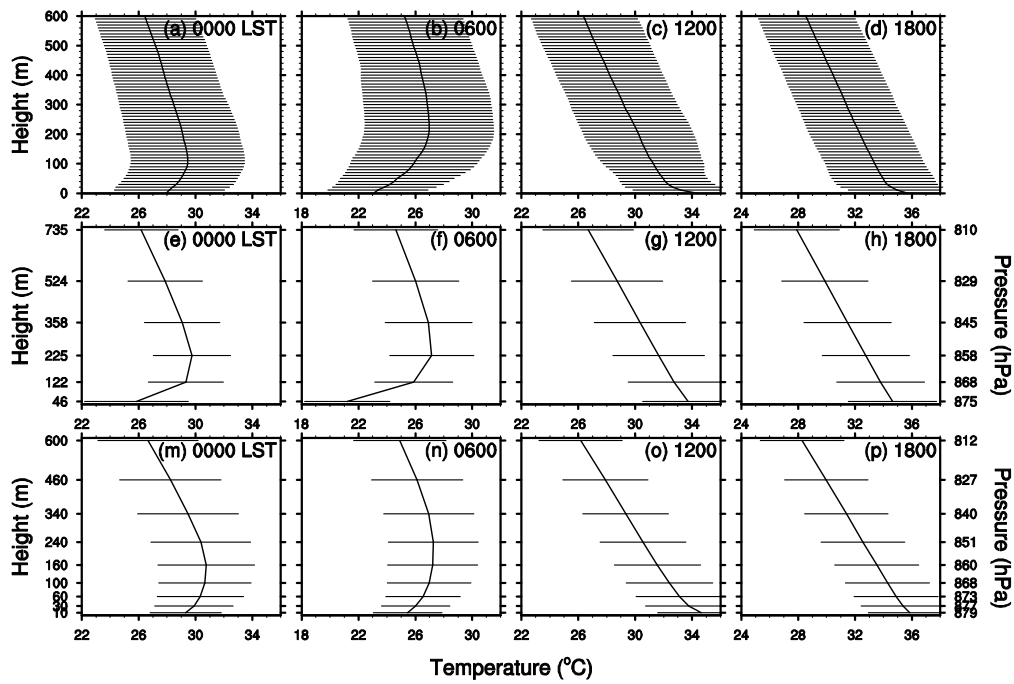
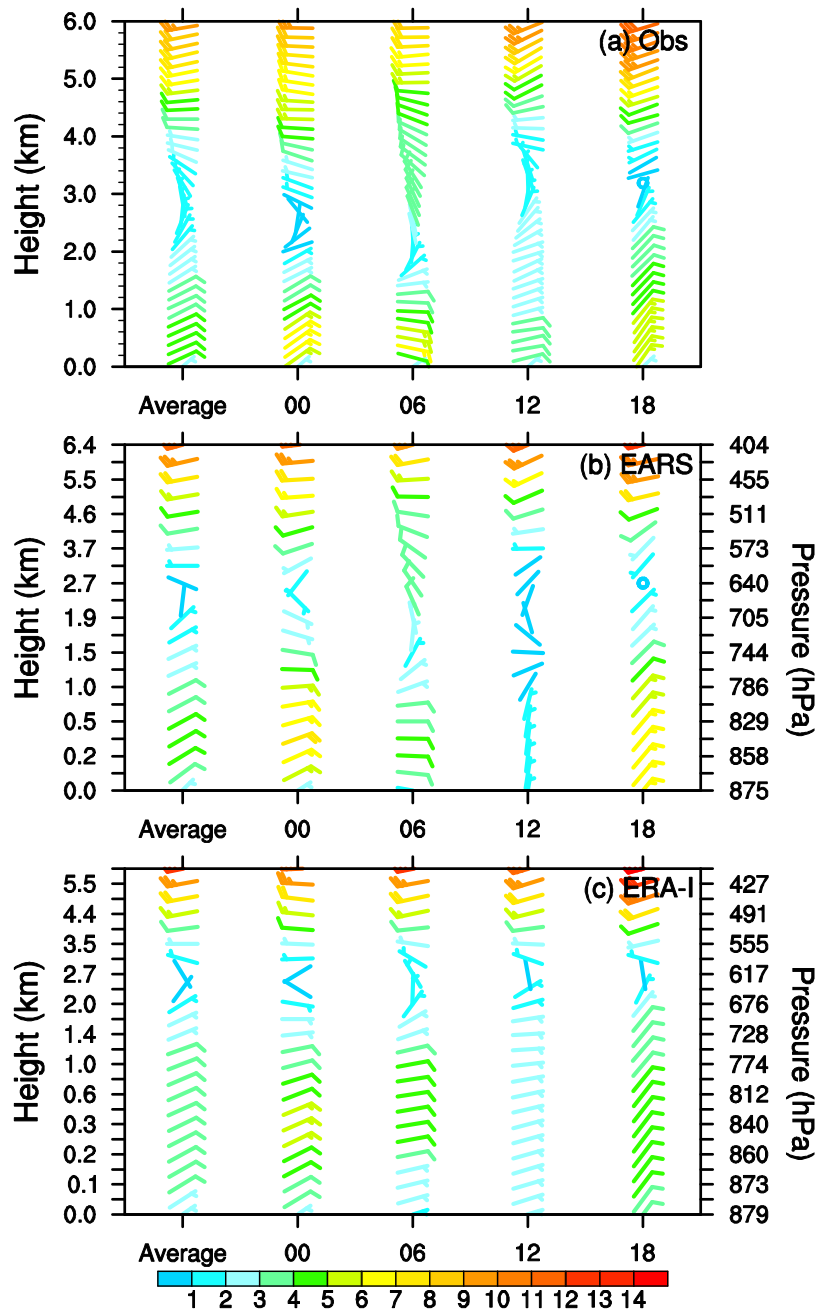


**Fig. 16** Diurnal transitions of the averaged temperature ( $^{\circ}\text{C}$ ) in lower levels from 0000 to 1800 local standard time (LST, = UTC + 6) in July 2016: (a) Observations (Obs), (b) EARS, and (c) EAR-I. Standard deviation at each level is marked.



860

**Fig. 17** Profiles of monthly-averaged horizontal wind barbs in July 2016: (a) observations (Obs), (b) EARS, and (c) ERA-I. A full wind barb denotes  $4 \text{ m s}^{-1}$ ; and the shading indicates horizontal wind speed ( $\text{m s}^{-1}$ ). Average denotes the total average of all times. Each column corresponds to the average profiles at 0000, 0600, 1200, and 1800 LST.

865